



Structural Assessment and Rehabilitation of an Existing Hydraulic Masonry Structure Supporting Railway

Aly A. Makhlof¹ , M. Omar¹, Dina A. Emarah^{1*}

¹ Construction Research Institute (CRI), National Water Research Center (NWRC), Delta-Barrage, 13621, Egypt.

Received 10 October 2024; Revised 17 January 2025; Accepted 21 January 2025; Published 01 February 2025

Abstract

Old hydraulic masonry structures are essential components of global road and rail infrastructures. Over decades of operation, these structures have experienced inevitable deterioration, necessitating evaluations of their structural conditions through comprehensive assessment and rehabilitation programs to ensure compliance with contemporary safety standards. This study focuses on a specific regulator as a case example to implement a rehabilitation strategy aimed at restoring its structural integrity after 190 years of continuous service. From 2015 to 2021, an extensive program was conducted to assess the condition of the construction materials. This program included mechanical and physical testing, as well as Finite Element Analysis (FEA), to identify areas of high stress and to analyze the distribution of stress throughout the structure. The findings revealed that the structure fails to meet current Egyptian standards, thereby underscoring the critical need for a strengthening program. Subsequently, a rehabilitation intervention was developed, which involved reinforcing the intrados of the arches and piers with a slender reinforced concrete jacket. These reinforcements were integrated with the existing structure using steel shear bar connectors. Following the rehabilitation, a re-evaluation of the analysis of the modified structure using FEA software confirmed compliance with Egyptian specifications. The proposed rehabilitation strategy offers a viable solution to the challenges associated with the examined masonry arch bridge.

Keywords: Hydraulic Masonry; Rehabilitation; Evaluation; Compressive Test; Strengthening.

1. Introduction

Hydraulic masonry structures, including regulators, culverts, dams, and masonry arch bridges, form the backbone of water management, transportation, and irrigation systems across the globe [1]. These structures, often constructed with exceptional engineering precision, have historically played critical roles in flood control, irrigation, and navigation [2]. Designed to withstand environmental stresses and operational demands over centuries, they are enduring symbols of human ingenuity and resilience [3]. However, the combined effects of aging, environmental degradation, and the increasing demands of modern infrastructure have intensified the challenges associated with preserving and maintaining these critical assets [4].

As infrastructure ages, the vulnerabilities of hydraulic masonry structures become increasingly apparent. Deterioration processes, including cracking, scouring, and material fatigue, are exacerbated by environmental factors such as moisture ingress, freeze-thaw cycles, and the effects of climate change. Fluctuating water levels, extreme flooding events, and prolonged exposure to hydraulic pressures have further accelerated their degradation [5, 6]. These issues are compounded in structures supporting modern railway systems, where dynamic loads from high-speed trains, heavier axle weights, and continuous vibrations often exceed their original design specifications [7]. The cumulative effect of these mechanical and environmental stresses compromises structural integrity, posing significant risks to safety, functionality, and long-term resilience [8, 9].

* Corresponding author: dina_emarah@yahoo.com

 <http://dx.doi.org/10.28991/CEJ-2025-011-02-012>



© 2025 by the authors. Licensee C.E.J, Tehran, Iran. This article is an open access article distributed under the terms and conditions of the Creative Commons Attribution (CC-BY) license (<http://creativecommons.org/licenses/by/4.0/>).

In response to these challenges, the field of structural assessment has evolved considerably. Traditional assessment methods relied heavily on visual inspections and basic structural tests and often failed to detect hidden vulnerabilities such as internal voids and micro-cracking. These tools allow for a comprehensive understanding of structural health by identifying internal material degradation, quantifying stress concentrations, and evaluating dynamic responses under operational loads [4, 9]. For example, Dynamic testing is a key method to check how well structures can handle changing loads. It helps identify problems, measure the impact of repairs, and ensure structures meet safety standards. This type of testing is especially useful for structures under forces like water flow, earthquakes, or trains, as it shows how they perform and helps extend their lifespan [7, 8].

The Finite Element Method (FEM) has emerged as an indispensable tool in structural assessment and rehabilitation planning, offering unmatched precision in analyzing the behavior of hydraulic masonry systems under a wide range of load scenarios. By simulating stress distributions, deformation patterns, and failure mechanisms, FEM empowers engineers to identify critical vulnerabilities and predict how structures respond to both dynamic and static loads, including extreme conditions such as seismic events, flooding, and heavy railway traffic. This capability makes FEM a cornerstone of modern diagnostic and intervention strategies, addressing both immediate and long-term challenges in structural management [10-12]. A major strength of FEM lies in its ability to integrate real-world data, such as material properties obtained from borehole sampling and mechanical testing, ensuring computational models closely align with the actual conditions of the structure. This precision enhances the reliability of analyses and supports the design of targeted, effective interventions. Additionally, FEM facilitates post-rehabilitation evaluations, simulating improved structural behavior to validate applied measures and ensure compliance with modern safety standards [13-15].

On a global scale, FEM has proven transformative in tackling issues faced by hydraulic masonry structures, including fluctuating hydraulic pressures, dynamic railway loads, and environmental degradation. Prominent examples like the Potenza railway bridge in Italy and the Waverley Mill Bridge in the UK highlight FEM's ability to guide effective rehabilitation strategies. These case studies demonstrate how advanced computational modeling, combined with real-world diagnostic data, can identify vulnerabilities, predict structural responses, and optimize intervention designs [7]. By addressing immediate deficiencies and establishing a replicable framework for sustainable management, FEM provides valuable insights for preserving hydraulic masonry structures worldwide, ensuring their resilience and functionality for future generations [16, 17].

The rehabilitation and strengthening of hydraulic masonry structures have similarly advanced, focusing on addressing the dual challenges of ensuring structural integrity and preserving historical significance [14, 15]. Over the years, a variety of methods, materials, and techniques have been employed to achieve these objectives. Among the innovative methods is the use of Fiber-Reinforced Polymers (FRPs), such as Glass Fiber Reinforced Polymer (GFRP) and Carbon Fiber Reinforced Polymer (CFRP). These materials enhance load-carrying capacity, increase ductility, and improve resistance to cracking under cyclic loads. For example, prestressed and non-prestressed GFRP bars have demonstrated significant improvements in ultimate strength and ductility when applied to masonry walls, highlighting their efficacy in absorbing energy and withstanding higher horizontal displacements [18-20]. Composite materials like Fabric-Reinforced Cementitious Matrix (FRCM) and Basalt-FRLM (Basalt Fiber-Reinforced Lime Mortar) have also gained popularity in rehabilitating historic structures due to their superior compatibility with masonry substrates and sustainability [21]. FRCM and Basalt-FRLM composites, applied to the extrados or intrados of masonry arches, have been shown to significantly enhance displacement capacity and ductility. These materials offer a balance between structural reinforcement and preservation of historical integrity, making them ideal for monuments and aged infrastructure. Techniques like steel fiber-reinforced mortar (SFRM) and advanced mortars are similarly effective, providing increased load-carrying capacity and ensuring a ductile response even under preloading conditions [22].

In parallel, grout injection has proven to be a valuable method for repairing fine cracks and voids in masonry structures, especially in water-retaining or hydraulic structures. Cement-based grouts, including microfine and mineral-enhanced formulations, restore the structural coherence and density of masonry piers while improving compressive strength and impermeability. Studies on barrages, such as Assiut and Naga-Hammadi in Egypt, demonstrated that grout injection improved compressive strength by over 80% and density by up to 8%, ensuring enhanced durability [23, 24]. The effectiveness of grout injection has been further validated through nondestructive techniques like acoustic tomography, ensuring optimal penetrability and quality assurance during restoration [24]. The application of Ultra-High-Performance Concrete (UHPC) and shotcrete in strengthening has also gained attention for its ability to improve masonry columns and surface resilience. UHPC confines masonry, preventing brittle failure and increasing compressive strength by up to 185%, while shotcrete is used to repair cracks and strengthen surfaces effectively [25]. Collectively, these methods provide an integrated framework for addressing the multifaceted challenges faced by hydraulic structures, ensuring safety, resilience, and sustainability while preserving historical significance [23-25].

Additionally, traditional techniques such as reinforced concrete jacketing, shotcrete linings, and injection grouting remain widely used and highly effective. Reinforced concrete jacketing increases the load-bearing capacity and resilience of critical structural components like piers and arches [26, 27]. Shotcrete offers a cost-effective solution for

repairing cracks and strengthening surfaces, while injection grouting restores cohesion within masonry joints, stabilizing the structure and preventing further degradation [28, 29].

The need for this study arises from the unique challenges posed by a 190-year-old hydraulic masonry regulator in Egypt. This structure, which manages water flow and supports a railway system, has been subjected to prolonged exposure to dynamic train loads and hydraulic pressures, resulting in significant structural deficiencies such as cracking, stress concentrations, and reduced load-bearing capacity. Between 2015 and 2021, a comprehensive investigation was conducted to assess the regulator's condition and develop a targeted rehabilitation strategy. Advanced diagnostics, including borehole sampling, dynamic testing, and FEM-based numerical simulations, were employed to identify critical vulnerabilities and inform intervention design.

The rehabilitation strategy included slender reinforced concrete jacketing, steel shear bar connectors, and shotcrete lining, integrated seamlessly into the existing masonry structure to enhance its durability and load-bearing capacity while preserving its historical character. One of the key objectives of this study is to utilize FEM analyses conducted both before and after rehabilitation to diagnose structural vulnerabilities, guide targeted interventions, and assess their potential effectiveness. The study aims to predict improvements in structural behavior by employing post-rehabilitation simulations, thereby evaluating the anticipated success of the applied measures in enhancing resilience and functionality under operational conditions.

By integrating mechanical and physical testing, FEM simulations, and sustainable rehabilitation techniques, this study contributes to the global discourse on preserving aging hydraulic masonry structures. The broader implications of this research extend beyond the Egyptian case study, providing a replicable model for addressing similar challenges worldwide. This study underscores the importance of combining modern engineering solutions with historical preservation, offering a proactive approach to ensuring the resilience and sustainability of critical infrastructure for future generations.

2. Material and Methods

2.1. Regulator Description

2.1.1. Location and Historical Background

Samalout Regulator is located at 219 + 078 km on the right side of the Ibrahimiya Canal right bank in Samalut - Minya Governorate, Egypt (Figure 1). It has proved impossible to correctly trace the construction history of this work due to inadequate information. It was built in 1834, crossing under the main Upper Egypt railway lines. The Regulator consists of two openings, each opening 2.60 m, as shown in Figure 2. There are two abutments with masonry arch rings. The piers were overlaid with a masonry arched bridge of 2.00 m thickness. The Red Clay Bricks have been used for construction with mortar. The Regulator was exposed to railway loads over two lanes. A standard gauge length of 1.435 meters was identified. Standard spacings and dimensions of the railway system are illustrated in Figure 3.



Figure 1. Regulator location Map ($28^{\circ}19'54.7''$ N, $30^{\circ}42'38.0''$ E)

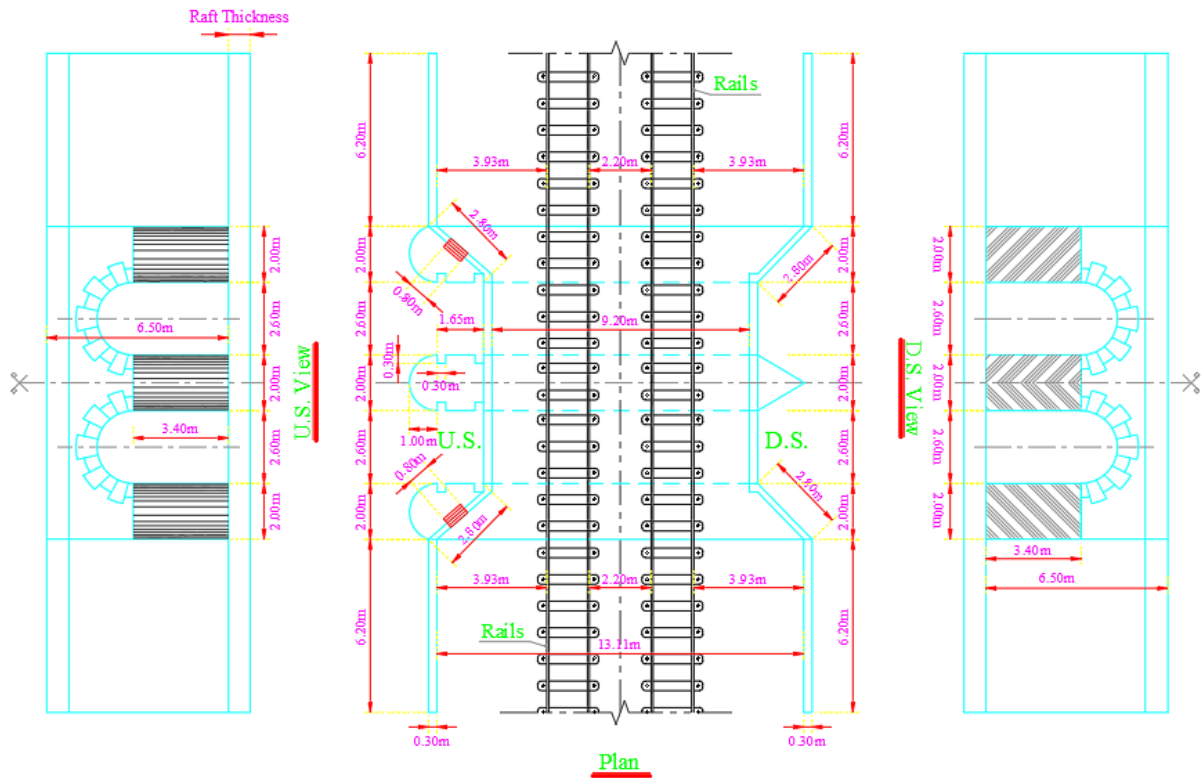


Figure 2. Current layout of the Regulator before rehabilitation works

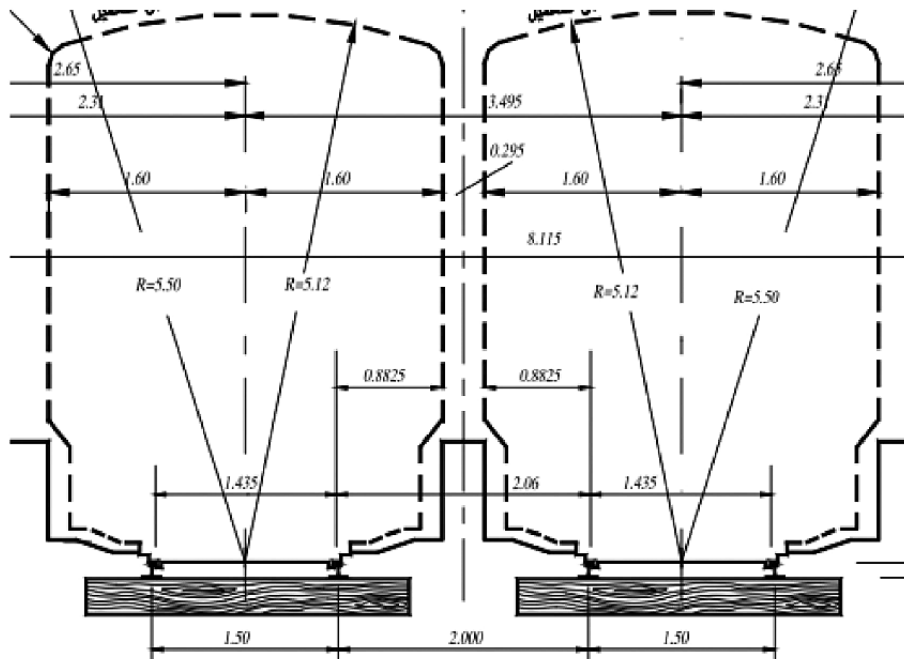


Figure 3. Standard spacing for the railway system (all dimensions are in meters) [30]

2.2. Material Evaluation

Figure 4 shows the framework of the process methodology and its implementation after developing the geometric representation of the masonry arch regulator. A visual inspection is conducted to determine the apparent condition of the regulator (Figure 5). Material properties of the constitutional material are extracted for material assessment. Continuous coring was conducted in two periods. Two reports addressed the test results of these samplings, dated 2015 and 2021, respectively. The Construction Research Institute team took samples, and tests were conducted according to the Egyptian Code for the Design and Implementation of Concrete Structures [31]. Figure 6 shows the obtained samples as well as the test configuration.

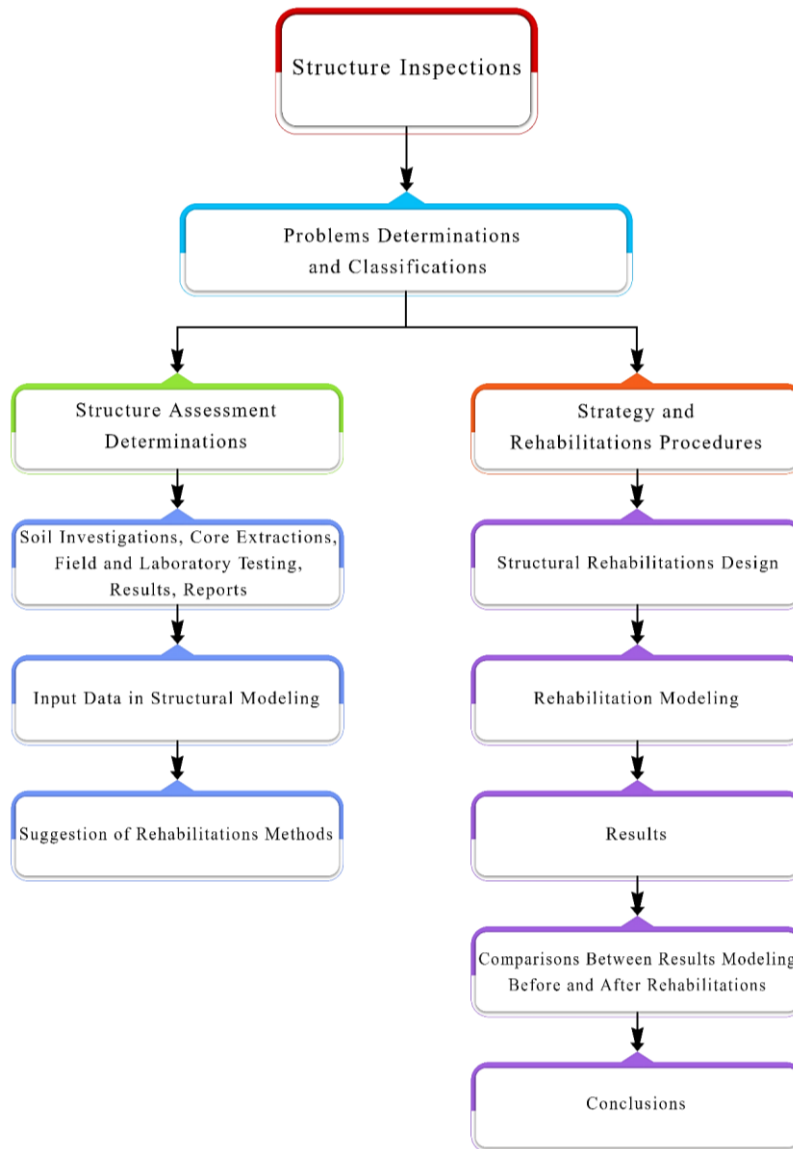


Figure 4. Frame work of the process methodology



Figure 5. Visual inspection conducted to assess the apparent condition of the Regulator

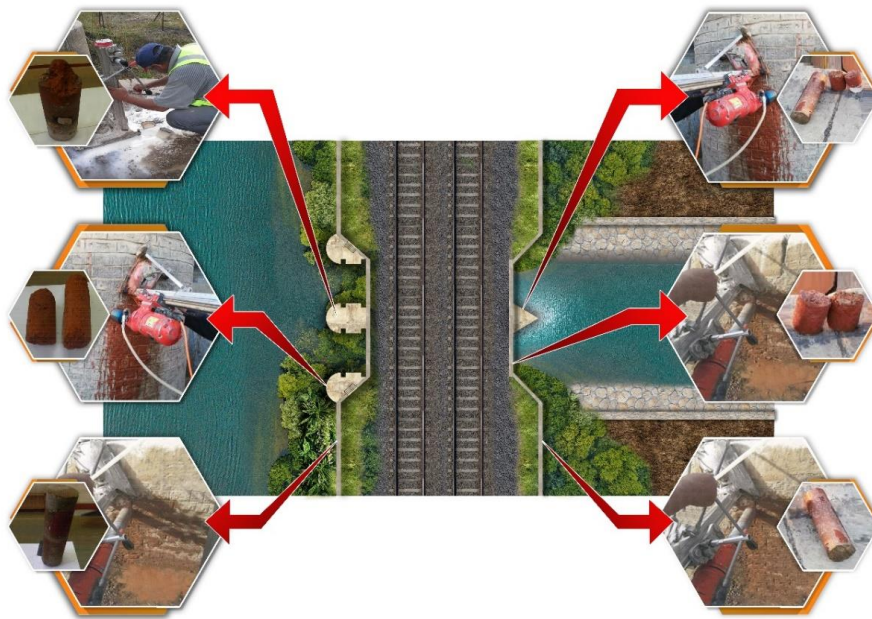


Figure 6. Concrete cores extracted from different locations through the Regulator

2.2.1. Natural Site Soil Investigation

The subsurface soil investigation, based on two boreholes drilled to a depth of 20.0 m below the site's surface, revealed a relatively homogeneous soil stratification across the investigated depth. The geotechnical profile consists of a 1.00 m thick filling layer at the surface, underlain by a silty clay layer with a thickness ranging from 6.00 m to 7.00 m, followed by a clayey sandy silt layer of 5.50 m to 6.50 m thickness. A sand layer, starting at 13.50 m, extends to the maximum investigated depth of 20.0 m. Groundwater was recorded at 4.00 m below the surface level during drilling. Standard Penetration Tests (SPT) were performed using a standard split-barrel sampler to evaluate in-situ soil strength, while laboratory tests followed the Egyptian Code for Soil Mechanics [32]. Direct shear tests on remolded sand samples determined the angle of internal friction, and unconfined compressive strength tests on undisturbed silty clay and clayey sandy silt samples provided the unit weight and cohesion values of the soils. The results recommended that transmitted stresses at the foundation level should not exceed 1.33 kg/cm^2 , with a modulus of subgrade reaction of $13,300 \text{ kN/m}^2/\text{m}$. The unit weight of dry soil samples ranged between 14.6 kN/m^3 and 17.5 kN/m^3 (average 16.2 kN/m^3), while the bulk density varied from 18.7 kN/m^3 to 21.9 kN/m^3 (average 20.7 kN/m^3). These findings, documented in the 2015 report by the Construction Research Institute (CRI), National Water Research Centre (NWRC), provide essential data for foundation design and construction, ensuring compliance with geotechnical standards and safety requirements.

2.2.1. Core Extraction Works

Several cores were extracted according to what is shown in Figure 6 so that they represent all the elements of the Regulator and are, therefore, distributed to different places in the Regulator. By observing the extracted cores, it became clear that a complete separation of the samples of some cores had occurred at the interval between the mortar and the bricks, as it was found that the thickness of the mortar appeared to be relatively large and, to a noticeable degree. The mortar used was Qasromil mortar (lime and brick-based mortar), as shown in Figure 7. The coring was done in two separate periods. Two reports addressed the findings of these samplings, dated 2015 and 2021, respectively, by the Construction Research Institute (CRI), NWRC.



Figure 7. Complete separation observed between the mortar and bricks in

2.3. Cores Compressive Strength

Before performing the test, the final dimensions of the different samples were measured after levelling each sample's ends so that the sample's lower and upper surfaces were perpendicular to the longitudinal axis of the sample, and capping was done if necessary. A compressive resistance test was conducted on those samples, followed by calculating the equivalent value of the compressive resistance of a standard cube of concrete samples according to the equation contained in Appendix Three of the Egyptian code for the design and implementation of concrete structures [31] (Guide to Laboratory Tests for Concrete Materials), at the same current age.

Figure 8 shows the test configuration. In 2015, the compressive strength tests of the tested cores showed that the compressive strength values of the tested samples ranged between 44.60 kg/cm^2 and 48.80 kg/cm^2 , with a total average of about 46.50 kg/cm^2 . In 2021, the compressive strength tests of the examined cores indicated that the compressive strength values of the samples varied from 41.08 kg/cm^2 to 47.63 kg/cm^2 , with an overall average of around 44.27 kg/cm^2 . The masonry unit weight samples vary from 16 to 18.5 kN/m^3 with an average value of 17 kN/m^3 . The deterioration rate in the year is 0.8%. Allowable tension strength is assumed to be no more than 10 %, considered compressive strength.



Figure 8. Compression test of core sample

2.4. Modeling Assumptions

Most of the antiquated barrages in Egypt were designed based on structural mechanics principles that did not account for the structures' three-dimensional behavior. The analysis relied on planar strain theory [13]. However, with advancements in understanding hydraulic systems, designers began to evaluate various loads affecting structural integrity. The application of finite element analysis (FEA) streamlined the design process and facilitated the calculation of local stresses within components and critical stress concentration points.

In this study, two phases of modeling were adopted: the first phase represented the Regulator with its original geometry, while the second simulated the Regulator after structural modifications to enhance its performance under different loading conditions. The raft was assumed to have a thickness of 2.20 m, with the core not penetrating the raft.

A 3D solid element model of the Regulator was developed using SAP2000 [33], incorporating all applied loads in accordance with the ECP 201 guidelines [30]. The masonry components, including the raft, abutments, wing walls, piers, and arches, were represented as a single-phase material through macro-modeling, where the brick units, mortar, and the interfaces between them were modeled as a smeared material, and the mortar joints were represented as zero-thickness interfaces. The gates were modeled as equivalent steel shell elements with dimensions of $0.5 \text{ m} \times 0.5 \text{ m}$, connected to the abutments and piers using link members.

The solid elements, being three-dimensional, were designed to represent the full thickness and volume of the structural components. Each element was assigned six degrees of freedom (DOF) per node: three translations and three rotations. The raft was modeled as a 2.20 m thick solid element, discretized into a mesh with an element size of $0.50 \text{ m} \times 0.50 \text{ m} \times 0.50 \text{ m}$. The materials were assumed to be linear, with the following properties: Young's modulus = $10,000 \text{ MPa}$, Poisson's ratio = 0.20, density = 17 kN/m^3 , and compressive strength = 44.27 kg/cm^2 , reflecting the experimental results for the brick material.

The abutments, wing walls, and piers were modeled on top of the raft using the same solid element size ($0.50 \text{ m} \times 0.50 \text{ m} \times 0.50 \text{ m}$) to ensure uniformity in the meshing strategy. Similarly, the arches were constructed on the abutments and piers using identical solid elements, maintaining consistency throughout the model. All solid elements were interconnected at joints to enable proper contact and stress transfer across the width and thickness of the regulator. The soil foundation was modeled as springs based on the Winkler assumption, with a spring stiffness (K) of $13,300 \text{ kN/m}^2/\text{m}$, derived from actual soil parameters.

Figures 9 and 10 illustrate the final stage of modeling the regulator with its original geometry. An envelope of the critical load combinations was generated and compared for both models, i.e., before and after strengthening. Water loads were applied as hydrostatic pressure, while the dynamic effects of water were modeled as equivalent static loads in accordance with the Egyptian code. Similarly, the dynamic earth pressure was represented as factored static loading as per the Egyptian foundation code [30]. The seismic loads were evaluated using the response spectrum analysis outlined in ECP 201 [30].

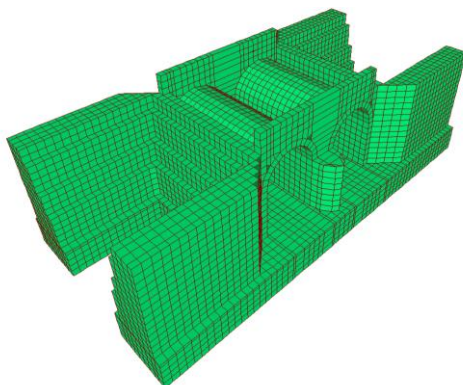


Figure 9. Finite Element Model (FEM) of the entire existing Regulator shape in the downstream direction

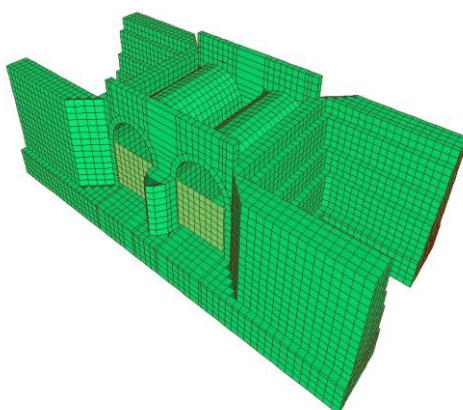


Figure 10. Finite Element Model (FEM) of the entire existing Regulator shape in the upstream direction

To simulate the operating conditions and new railway loads, the Finite Element Model (FEM) was subjected to normal operating loads, railway breaking forces, and seismic loads. For massive sections where small deformations were expected, linear modeling was utilized to identify the most stressed regions of the Regulator. Earth pressure was modeled using equivalent static loading, and the effects of uplift pressure, maintenance forces, and impact forces were incorporated (Figure 11). These forces included P1: surcharge, P2: earth pressure (static and dynamic), P3: uplift pressure, P4: water pressure (static and dynamic), W1: weight of soil layer above the arch, and W live load: train live load. Uplift pressure was treated as equivalent to static pressure.

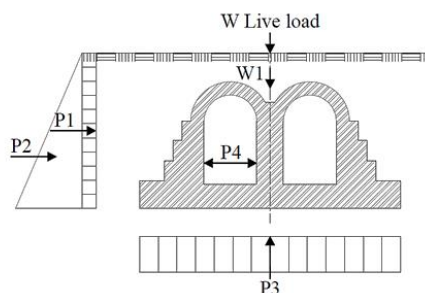


Figure 11. Case loading of the Regulator

To simulate the railway impact, a train model was introduced (Figure 12), assuming the locomotive's mass to be 122 tons. The results provided insights into the stress distribution and performance of the Regulator under existing and new loading conditions, further validating the structural modifications and their compliance with modern design standards.



Figure 12. Train model weighing 122 ton

The loads acting on the Regulator structure were calculated according to ECP 201 [30] and can be listed as follows according to Egyptian code (Equations 1 to 9):

- Dead load: the own weight of the structural element and the fill material till the road surface.
- Train equivalent loads as per Egyptian code (Figure 13).
- The train load impact factor as per ECP 201 [30] is calculated from the following equation:

$$I = 0.73 + \frac{2.16}{\sqrt{L_I - 0.2}} - 1 \tag{1}$$

where I is Impact factor, (0.1 < I < 1.0). For arch bridges:

$$L_I = 0.5 l \text{ (for arch bridges)} \tag{2}$$

where L_I is Effective length for calculation impact factor, and l is Bridge span. After substitution in the equations:

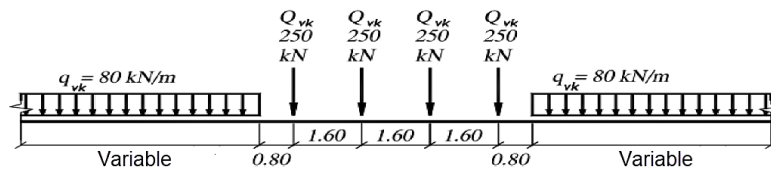


Figure 13. Train equivalent loads - load model 71

- Water Loads:
 - a) The effect of static water pressure on piers, abutments, and raft which is calculated according to ECP 202 [32] using the following equation:

$$P_w = \gamma_w * h \tag{3}$$

where: γ_w is water density, and h is depth of water.

- b) The effect of dynamic water pressure which is calculated according to ECP 202 [32] using the following equation:

$$P = C_s * C_h * \gamma_w * h \tag{4}$$

As for the coefficient C_s , it can be calculated using the following equation:

$$C_s = \frac{C_m}{2} \left[\frac{y}{h} \left(2 - \frac{y}{h} \right) + \sqrt{\frac{y}{h} + \left(2 - \frac{y}{h} \right)^2} \right] \tag{5}$$

where C_h is Horizontal seismic factor, h is Height of water, y is Distance from water level, and C_m is Maximum value of C_s factor, which is determined from ECP 202 [32].

- Earth Pressure Effect:
 - a) The effect of static earth pressure on the abutment and wing walls is deduced from the equation:

$$P = \gamma_s * K_a * h_s \tag{6}$$

where γ_s is Soil density, $K_a = \frac{1 - \sin\phi}{1 + \sin\phi}$ (where ϕ = The friction angle of soil), and h_s is Depth of soil column.

- b) The effect of dynamic earth pressure from ECP 202 [32] is calculated using the following equation:

$$P_{as} = \gamma_s * h * K_{as} \tag{7}$$

where P_{as} is Total load resulting from the seismic lateral pressure per unit length of the wall, γ_s is Unit weight of the soil, h is Height of the soil behind the wall, and K_{as} is Coefficient of seismic lateral earth pressure.

The coefficient of seismic lateral earth pressure for soil under seismic impact is calculated using the following equation:

$$k_{as} = \frac{(1 \pm c_v) \cos^2(\Phi - \lambda + \alpha)}{\cos \lambda * \cos 2\alpha \cos(\delta + \lambda - \alpha)} * \left[\frac{1}{1 - \left(\frac{\sin(\Phi + \delta) \sin(\Phi + i - \lambda)}{\cos(\alpha - i) \cos(\delta - \alpha + \lambda)} \right)^{0.5}} \right]^2 \tag{8}$$

where Φ is Internal friction angle of the soil, α is the angle of inclination of the ground surface from the horizontal, δ is The angle of friction between the soil and the wall, and $\lambda = A$ factor dependent on the seismic coefficients c_h and c_v , calculated according to the following equation:

$$\lambda = \tan^{-1} \frac{c_h}{1 \pm c_v} \tag{9}$$

- Seismic loads for zone 1 as per ECP 201 [30] which is compatible with the European code. For zone 1: seismic acceleration (a_g) = 0.1g, import factor (I) = 1.3, subsoil class = D, Design response spectrum = Type 1, and Mass = Dead Loads + 0.3 Live Loads.

2.5. Analysis Results

This section presents the results of the Finite Element Method (FEM) analysis, providing a detailed evaluation of the Regulator's structural performance under both static and dynamic loading conditions. The primary goal was to assess stress levels across critical cross-sections of the structure and identify areas that require rehabilitation and repair.

2.5.1. Normal Stress Distribution

Figures 14 and 15 illustrate the normal stress distribution along critical cross-sections in the x- and y-directions under normal operating conditions. In the x-direction (Figure 14), elevated stress concentrations were observed around the central portions of the arches and specific sections of the abutments. The analysis of the raft indicates that its entire height remains in compression, with compressive stresses reaching 1.4 kg/cm². However, tensile stresses as high as 5.80 kg/cm² were observed at the sides of the raft beneath the abutments, exceeding the allowable masonry tensile strength. These findings are consistent with the field measurements by Anwar et al. [8], who reported maximum tensile stresses of 2.7 kg/cm² at the base of walls. Additionally, tensile stresses at the top of the raft at the centre of the regulator opening reached 2.85 kg/cm².

The abutments showed compressive stresses throughout their height, reaching 1.4 kg/cm², while the piers exhibited compressive stresses ranging from 1.4 to 5.14 kg/cm². In the arches, compressive stresses varied between 1.4 and 3.80 kg/cm² near the crown, whereas maximum tensile stresses of 4.70 kg/cm² were observed at the bottom near the arch crown, surpassing the allowable masonry tensile strength. These results align with Anwar et al. [8], who also reported critical tensile and compressive stresses in similar structures.

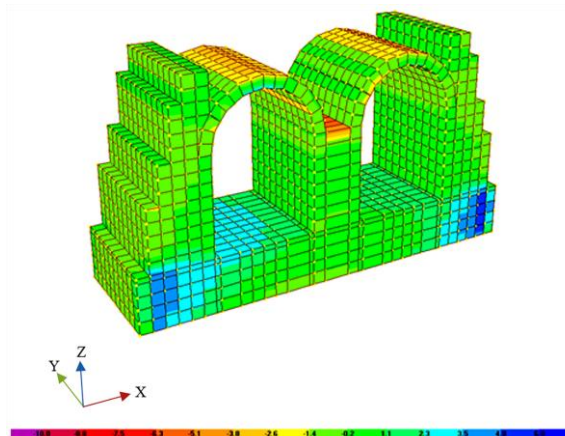


Figure 14. Maximum stresses in the original structure due to static and dynamic loading along x-direction (kg/cm²)

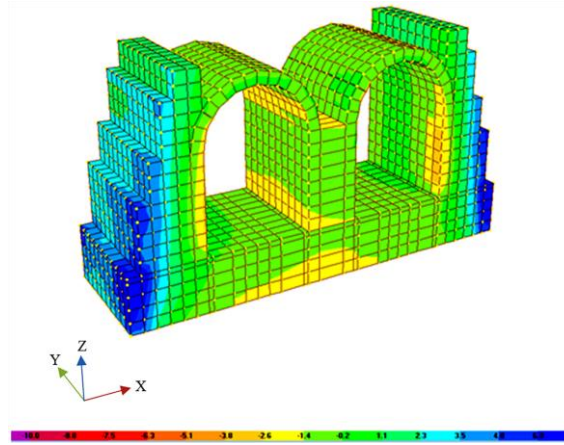


Figure 15. Maximum stresses in the original structure due to static and dynamic loading along y-direction (kg/cm²)

In the y-direction (Figure 15), significant stress concentrations were observed around the abutments and the base of the structure. Tensile stresses in the raft beneath the abutments peaked at 5.80 kg/cm², while tensile stresses at the top of the raft reached 2.30 kg/cm², far exceeding the 0.7 kg/cm² reported by Anwar et al. [8] for similar cases. The abutments also experienced tensile stresses of 5.80 kg/cm², further exceeding safe limits. No tensile stresses were observed in the piers, where compressive stresses peaked at 2.60 kg/cm². Meanwhile, compressive stresses in the raft, arches, and abutments remained below allowable limits, confirming the findings of Anwar et al. [8] regarding compression stress distribution. The analysis highlights that the tensile stresses in the raft, abutments, and arches exceed allowable masonry tensile strength, posing a risk of cracking and structural deterioration. Specifically, tensile stresses peaked at 4.54 kg/cm² in the arches and 5.80 kg/cm² in the abutments, emphasizing the need for targeted strengthening measures. In contrast, the stress levels in other structural elements, such as piers and wing walls, were found to be within acceptable limits.

Figures 16 to 19 provide detailed visualizations of the maximum tensile and compressive stresses under static and dynamic loading for the raft, arch, pier, and abutments, respectively. Table 1 summarizes the tension and compression stresses in various components before any strengthening measures were taken.

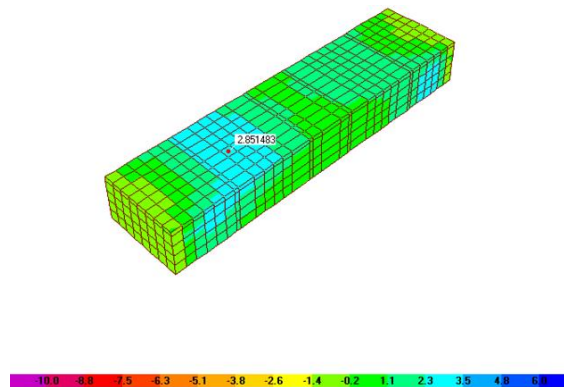


Figure 16. Maximum stresses (kg/cm²) in the original raft due to static and dynamic loading

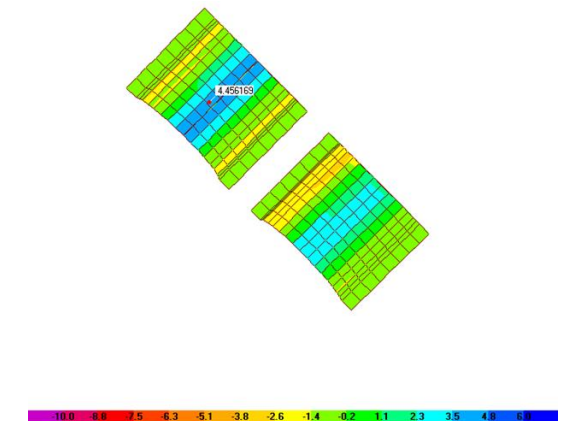


Figure 17. Maximum stresses (kg/cm²) in the original bottom of the arch due to static and dynamic loading in the original state (kg/cm²)

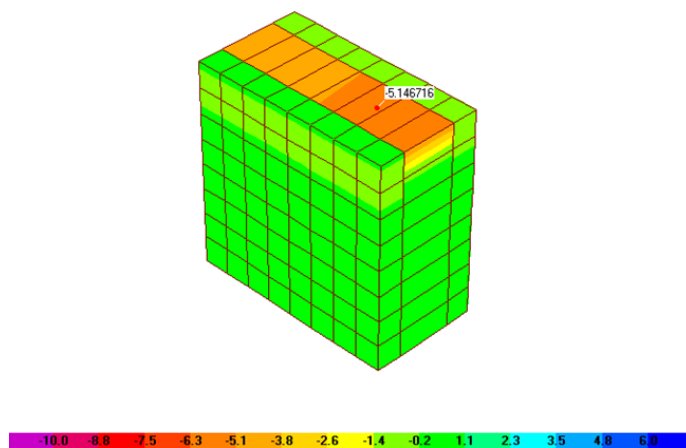


Figure 18. Maximum stresses (kg/cm²) in the original pier due to static and dynamic loading in the original state

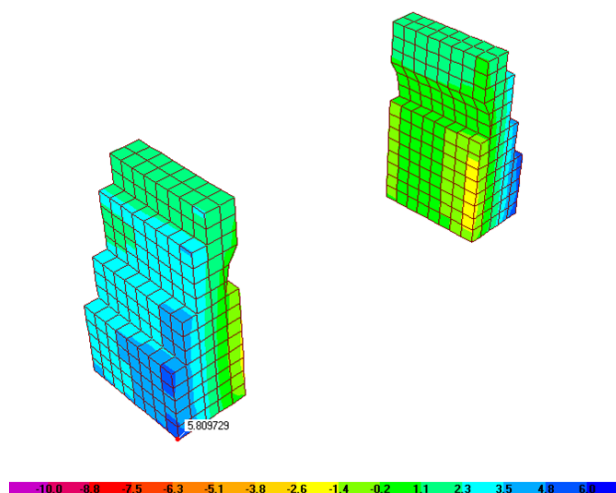


Figure 19. Maximum stresses (kg/cm²) in the original abutment due to static and dynamic loading in the original state

Table 1. Values of tension and compression stresses before strengthening

No.	Element	Material	Tension (kg/cm ²)	Compression (kg/cm ²)
1	Raft	Brick	2.85	0.50
2	Arch	Brick	4.54	2.83
3	Abutment	Brick	5.80	0.90
4	Pier	Brick	0.00	5.14

In the raft (Figure 16), tensile stresses reached 2.85 kg/cm², while compressive stresses remained at 0.50 kg/cm², both within acceptable limits. However, in the arches (Figure 17), tensile stresses at the bottom near the arch crown peaked at 4.54 kg/cm², accompanied by compressive stresses of 2.60 kg/cm², which aligns with observed cracking and mortar deterioration in this region. The piers (Figure 18) exhibited maximum compressive stresses of 5.14 kg/cm², with no tensile stresses recorded. Finally, in the abutments (Figure 19), tensile stresses reached 5.80 kg/cm², while compressive stresses were 2.60 kg/cm², reinforcing the conclusion that tensile stresses in these regions exceed allowable limits and require reinforcement.

The findings from the FEM analysis emphasize the critical stress concentrations in the arches and abutments, where tensile stresses surpass allowable masonry limits. These results necessitate targeted reinforcement efforts to address elevated stress levels, prevent cracking, and enhance structural resilience. Comparisons with Anwar et al. [8] further validate the observed stress distribution trends, highlighting the need for rehabilitation to ensure the long-term stability and functionality of the structure.

2.5.2. Shear Stress Distribution

Figures 20 and 21 show shear stress distribution among a critical cross-section of the Regulator under normal operating conditions – S1-2 and S1-3 directions, respectively. High shear stress was recorded in the arch (2.99 kg/cm²),

while other components like the abutment and pier have lower shear stress levels (0.35 kg/cm² and 0.46 kg/cm², respectively). The data in Table 2 provide a concise view of maximum shear stress values across the regulator's elements before any reinforcement measures. These values highlight the need to prioritize the arch for strengthening due to its elevated shear and tensile stresses.

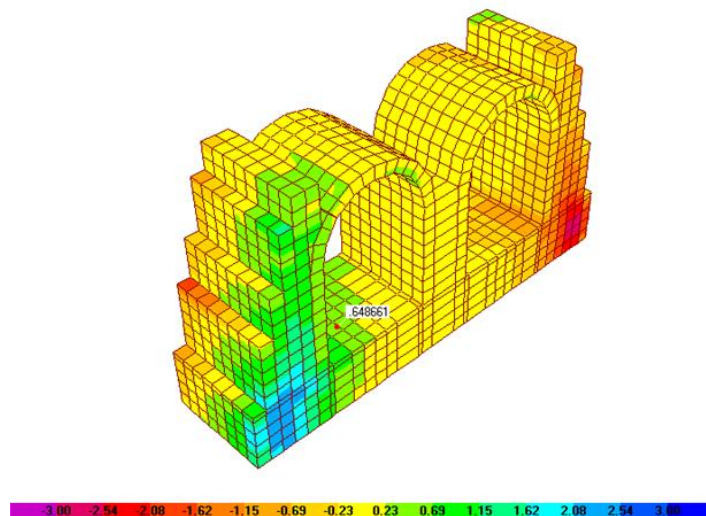


Figure 20. Maximum shear stresses (S1-2) in the original bricks Regulator due to static and dynamic loading in the original state (Kg/cm²)

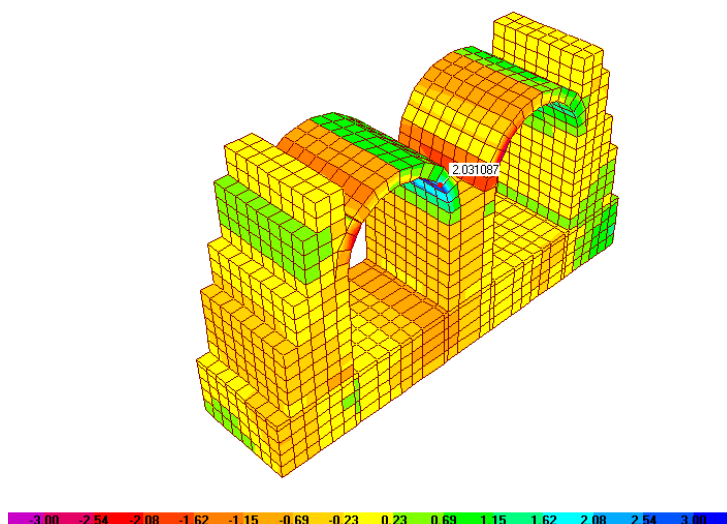


Figure 21. Maximum shear stresses (S1-3) in the original bricks Regulator due to static and dynamic loading in the original state (kg/cm²)

Table 2. Values of shear stresses before strengthening

No.	Element	Material	Shear Kg/cm ²
1	Raft	Brick	0.91
2	Arch	Brick	2.99
3	Abutment	Brick	0.35
4	Pier	Brick	0.46

3. Structural Rehabilitation Design

Traditional strengthening techniques, such as the unstitch-stitch method and mortar injection, are commonly applied to masonry bridges to address degradation in structural elements and mortar joints. However, these methods often fail to provide sufficient capacity to withstand modern external loads. For masonry arch structures, a common approach involves using tie rods at the springing points to absorb the horizontal thrusts generated by the arch shape [34]. While effective, tie rods can be aesthetically and functionally unsuitable, particularly for bridge structures. Historically, temporary support techniques, such as applying steel or wooden centering to the arch intrados, were also employed.

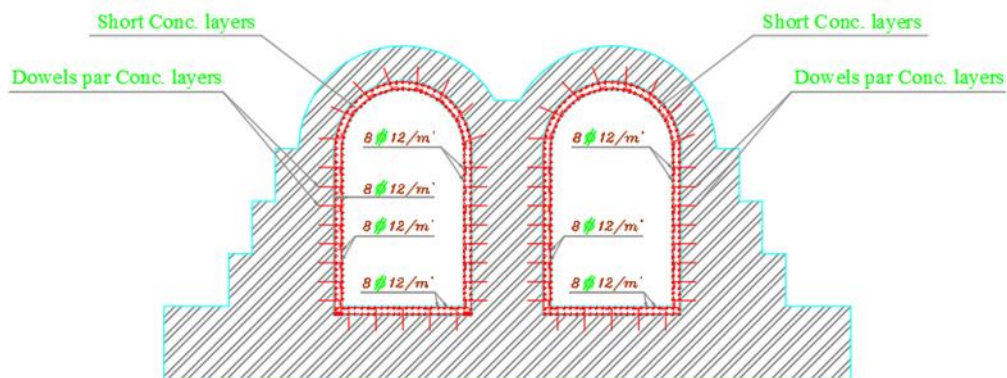
In recent years, traditional strengthening techniques have been largely replaced by more innovative methods, particularly the use of composite systems such as Fiber-Reinforced Polymers (FRPs) and Fabric-Reinforced Cementitious Matrix (FRCM) at the intrados, which contribute tensile strength to the masonry [35–40]. These solutions, due to their physical and mechanical compatibility with historical masonry, enhance both the strength and ductility of the structure.

Mohamed et al. [13] proposed methods for upgrading hydraulic regulators. One method involves increasing the raft thickness by adding concrete blocks, with shear dowels placed between the raft and the added blocks to ensure composite action between the two segments. Alternatively, the overstressed part of the raft can be replaced with reinforced concrete without increasing the raft thickness. However, this method requires dewatering the regulator and reducing the uplift forces acting on it during repairs. The replaced part remains vulnerable to uplift forces, necessitating the study and implementation of artificial systems to mitigate these forces during construction. Lowering the upstream water level is another effective strategy for reducing uplift forces.

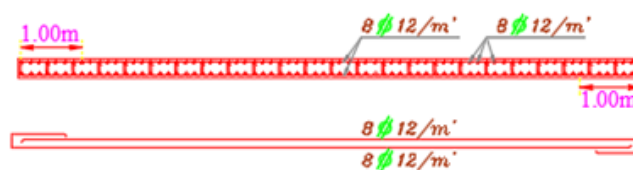
A previous attempt to repair cracks in the arch of the Samalout Regulator, located in Samalut, Minya Governorate, Egypt, using mortar injection, proved unsuccessful. In such cases, modern and efficient retrofitting systems are required to enhance structural strength and stiffness. One effective approach involves casting a reinforced concrete (RC) cover on the arch intrados after anchoring it to the existing structure.

This study demonstrates the effectiveness of integrating reinforced concrete (RC) jacketing, steel shear bar connectors, and shotcrete linings to address the structural deficiencies of a 190-year-old hydraulic masonry regulator. Unlike traditional methods such as mortar injection or the unstitch-stitch technique, which are limited in addressing large-scale deficiencies and dynamic loads, the RC jacket redistributes tensile and compressive stresses, significantly enhancing structural resilience. While modern solutions like Fiber Reinforced Polymers (FRPs) offer high strength-to-weight ratios and durability, they are often cost-prohibitive and impractical for large-scale applications. By balancing cost-effectiveness, compatibility with historical materials, and validation through Finite Element Modeling (FEM), this approach ensures long-term durability and compliance with modern safety standards, offering a replicable model for strengthening aged masonry hydraulic structures under contemporary operational demands.

In this study, the rehabilitation program included constructing an internal RC jacket for the raft, abutment walls, piers, and arches. Before concrete placement, all surfaces were thoroughly cleaned to remove oil, standing water, mud, loose rock, and debris. Cracks were cleaned, moistened, and injected with high-adhesion mortar. Grooves, 200 mm deep and spaced 500 mm apart in both directions, were drilled into the raft, walls, and arches. Steel bars with a diameter of 16 mm ($\text{\O}16$) were chemically anchored into these grooves using a non-shrink cement-based adhesive. Subsequently, a 200 mm thick RC jacket was installed, reinforced with upper and lower layers of steel mesh ($8 \text{ \O}12/\text{m}^2$), as depicted in Figure 22.



(a) RC jacket details



(b) RC details of walls

Figure 22. Reinforced concrete details

The concrete was poured in phases, starting with the raft, followed by the abutment walls, and shotcrete was applied in two layers for the arches. The arches and walls were finished with 20 mm cement plaster and coated with epoxy paint for additional protection. The RC jacket and shotcrete mix design included 450 kg/m³ of Sulfate Resisting Cement (SRC), crushed basalt as coarse aggregate, and natural sand with a specific gravity of 2.6 as fine aggregate. The sand-to-total aggregate ratio was 0.50 for reinforced concrete and 0.28 for shotcrete, with a water-to-cementitious materials ratio (w/cm) of 0.44. A high-performance superplasticizer (Addicrete BVF) was used to achieve the required workability, while Sika Control minimized dry shrinkage, and Addicrete DM2 was added as a waterproofing admixture. Compressive strength tests conducted on 24 concrete cubes (150 mm × 150 mm × 150 mm) at 7 and 28 days, following ECP 203 standards [31], confirmed the reliability of the RC jacket in improving the structure’s strength and stiffness. This comprehensive intervention significantly enhanced the structural integrity of the regulator, providing an effective and durable solution for retrofitting masonry arch structures to meet current operational demands. Table 3 represents the concrete mix proportions per cubic meter, Figure 23 outlines the steps involved in the structure rehabilitation process, Figure 24 shows the structure after rehabilitation, and Figure 25 highlights the average compressive strength of reinforced concrete and shotcrete lining. This was reported by the Construction Research Institute (CRI), National Water Research Centre (NWRC), dated 2023.

Table 3. Concrete mix proportions per cubic meter

Concrete Mix	Sulfate resisting cement (kg)	Crushed Basalt (kg)	Sand (kg)	Water (Litre)	Addibond 65 (kg)	Addicrete DM2 (kg)	Addicrete BVF (kg)	SiKa Control (kg)
Reinforced concrete	450	1360	680	200	---	---	---	2
Shotcrete	450	2400	680	200	4	4	8	2



Figure 23. Structural rehabilitation



Figure 24. Structural after rehabilitation

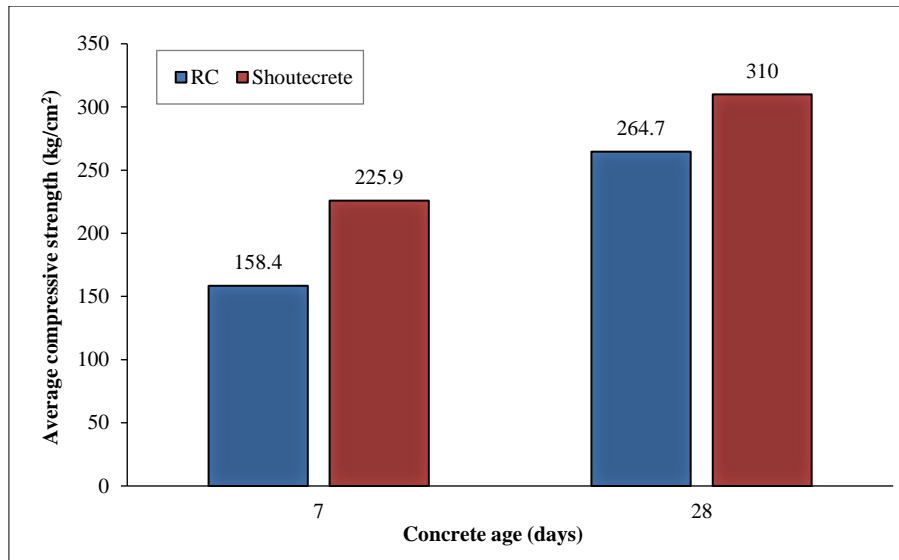


Figure 25. Average compressive strength of reinforced concrete and shotcrete jacket

3.1. Rehabilitation Modeling Assumption

The second model simulated the Regulator after the implementation of rehabilitation structural modifications designed to enhance its performance under new loading conditions. The reinforced concrete (RC) jacket was modeled as a 0.50 m × 0.50 m × 0.20 m solid element mesh, with material properties assigned based on the rehabilitation program design. These properties included Young's modulus = 22,000 MPa, Poisson's ratio = 0.20, density = 24 kN/m³, and concrete compressive strength = 260 kg/cm². Figures 26 and 27 illustrate the final stage of the Regulator's modeling after the rehabilitation modifications.

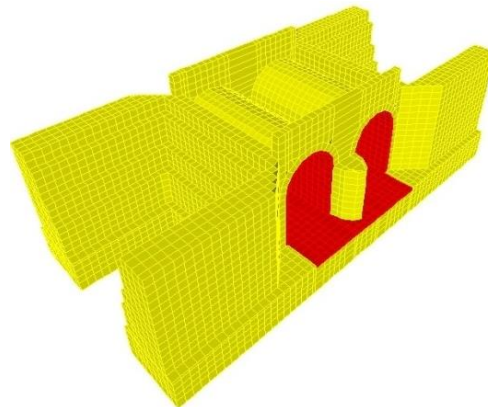


Figure 26. Finite Element Model (FEM) of the entire Regulator shape after strengthening in the downstream direction

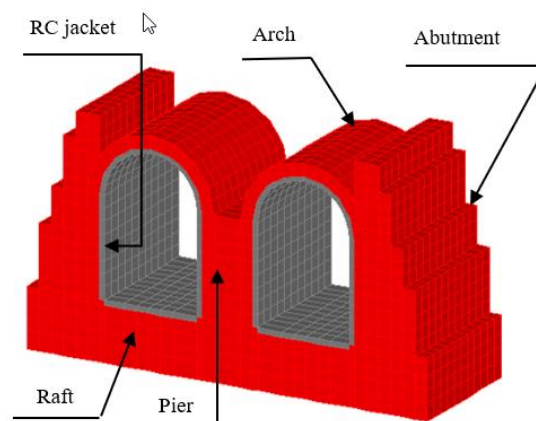


Figure 27. Finite Element Model (FEM) for the Cross-section strip of the Regulator after strengthening

3.2. Results of Rehabilitation

Before strengthening, the Regulator was subjected to various stresses that it could only manage to a limited extent due to the inherent properties of brick. While brick performs well under compression, it is less effective at resisting tensile and shear stresses, which compromises the long-term durability and safety of structures under varying loads. To address these limitations, the strengthening process included increasing the thickness of the raft, walls, and arch, along with the application of a reinforced concrete (RC) jacket. This intervention effectively redistributed normal stresses compared to the original stress distribution, as presented in Table 4 and illustrated in Figures 28 and 29. The rehabilitation work commenced on June 19, 2023, and was successfully completed by August 23, 2023.

Table 4. Values of tension and compression stresses after strengthening

No.	Element	Material	Tension (kg/cm ²)	Compression (kg/cm ²)
1	Raft	RC	5.54	0.00
2	Arch	RC	6.62	2.02
3	Abutment	RC	0.90	8.80
4	Pier	RC	0.00	0.69
5	Raft	Brick	1.77	0.00
6	Arch	Brick	0.63	2.04
7	Abutment	Brick	4.54	0.70
8	Pier	Brick	0.00	1.60

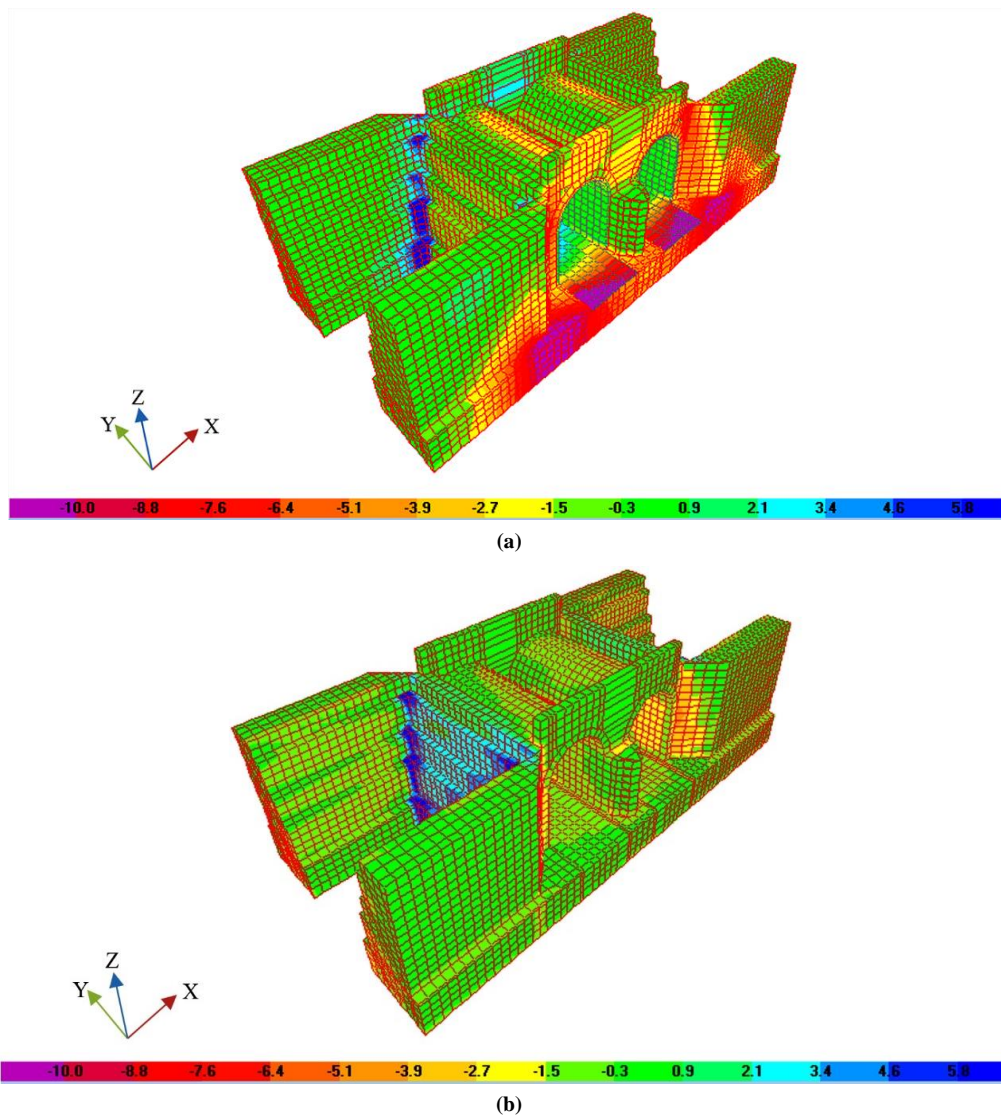


Figure 28. a) Maximum stresses (kg/cm²) in strengthened arch, wall, pier and raft due to static and dynamic loading after strengthening along the x-direction, b) Maximum stresses (kg/cm²) in strengthened arch, wall, pier and raft due to static and dynamic loading after strengthening along the y-direction.

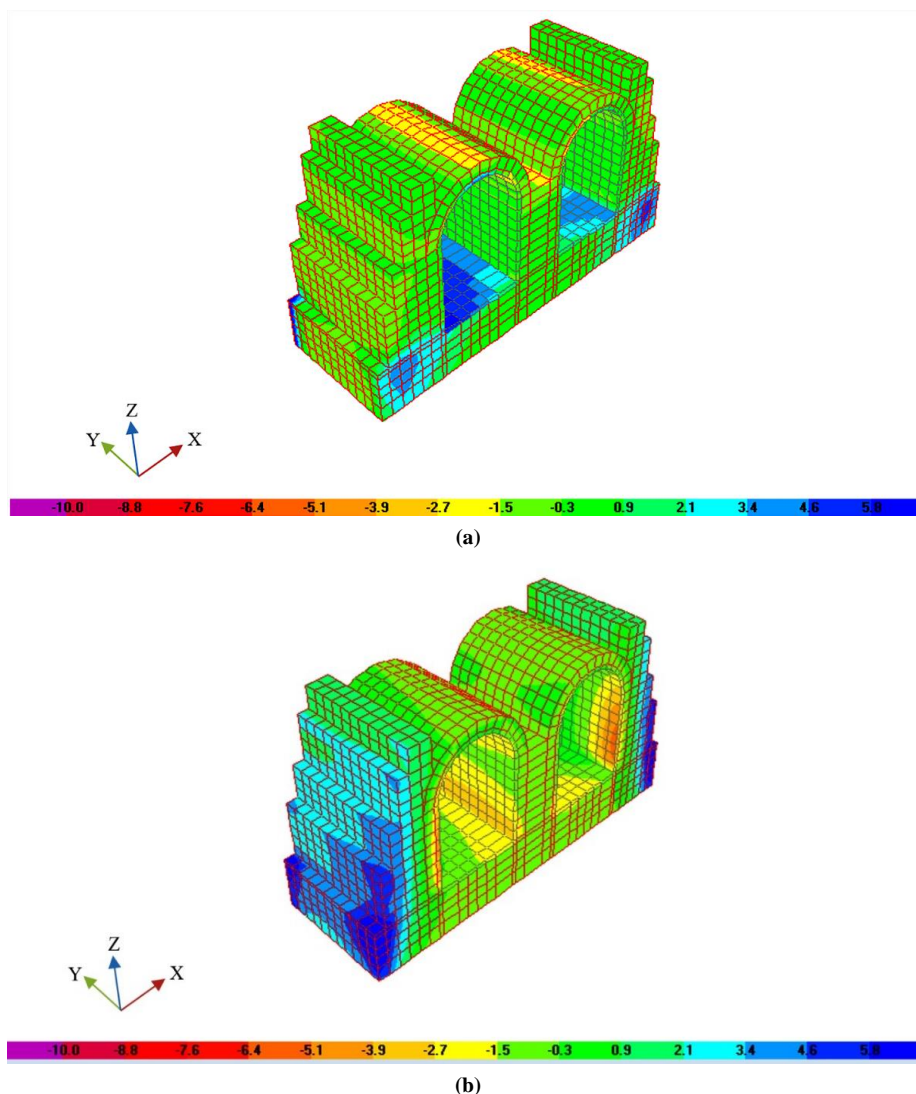


Figure 29. a) Maximum stresses (kg/cm^2) in RC and bricks strip due to static and dynamic loading after strengthening along the x-direction, b) Maximum stresses (kg/cm^2) in RC and bricks strip due to static and dynamic loading after strengthening along the y-direction.

Post-strengthening analysis revealed a significant reduction in critical stress levels across key structural elements. Figure 28-a shows the normal stress distribution in the x-direction, where the wing wall and raft remained in compression, with compressive stresses of approximately 1.4 kg/cm^2 in the wing wall and 10 kg/cm^2 in the raft. In the y-direction (Figure 28-b), no tensile stresses were observed, with maximum compressive stresses recorded at 6.7 kg/cm^2 in the wing wall and 12 kg/cm^2 in the raft, both within acceptable limits relative to the allowable masonry compressive strength.

Figure 29-a presents the normal stress distribution in the x-direction for the abutment, raft, pier, and arches. The abutment and pier were entirely in compression, with compressive stresses of around 1.5 kg/cm^2 . However, the arches exhibited maximum compressive stresses of 2.7 kg/cm^2 at the top and tensile stresses of 3.4 kg/cm^2 at the bottom. Local tensile stresses of 4.4 kg/cm^2 were also noted under the abutment in the raft, while the remainder of the raft remained primarily in compression. In the y-direction (Figure 29-b), compressive stresses reached 5.1 kg/cm^2 in the abutment and pier and 1.5 kg/cm^2 in the raft and arches.

Following strengthening, the maximum tensile stress in the raft bricks was reduced to 1.78 kg/cm^2 (Figure 30), while the bottom of the arches recorded a maximum tensile stress of 0.63 kg/cm^2 (Figure 31). The compressive stresses in the pier remained below the allowable masonry compressive strength (Figure 32). In the abutment, the maximum tensile stress reached 4.54 kg/cm^2 (Figure 33). Table 4 confirms that the reinforced components achieved improved load distribution, reducing tensile stresses in critical areas to 0.63 kg/cm^2 in the arch bricks, 1.77 kg/cm^2 in the raft, and 4.54 kg/cm^2 in the abutment. These results are consistent with the findings of Bancardino et al. [7], who evaluated the seismic vulnerability of a masonry arch bridge on the San Nicola–Avignano Lucania line using nonlinear static pushover analysis. Their study demonstrated that traditional rehabilitation techniques, such as jacketing and linings, effectively enhanced seismic performance, ensuring compliance with modern code requirements.

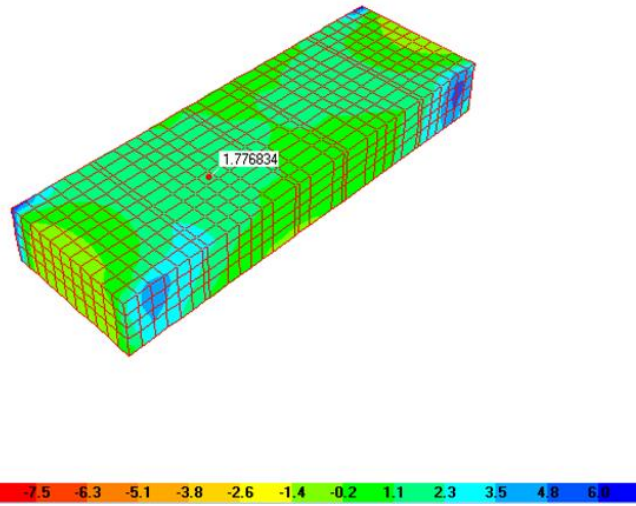


Figure 30. Maximum stresses (kg/cm²) in bricks strip due to static and dynamic loading after strengthening

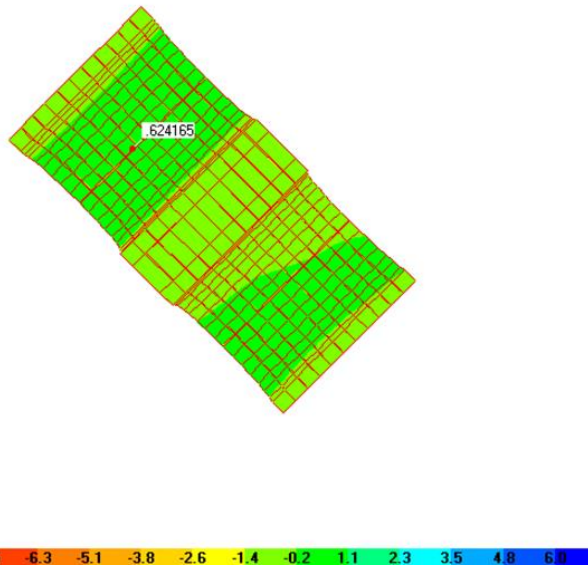


Figure 31. Maximum stresses (kg/cm²) in the strengthened bottom of the brick arch due to static and dynamic loading after strengthening

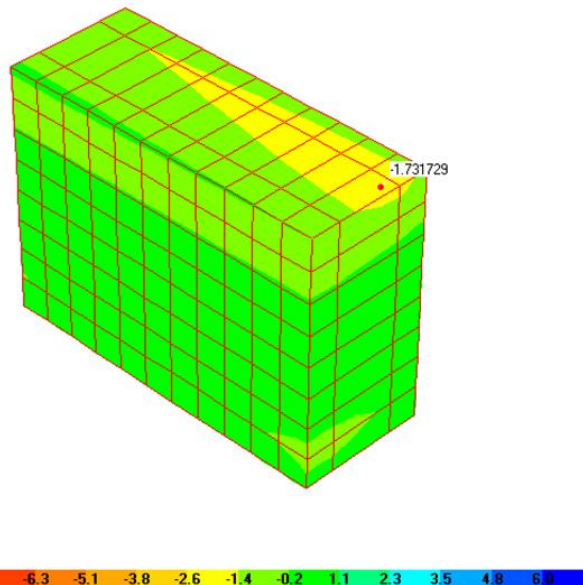


Figure 32. Maximum stresses (kg/cm²) in the strengthened brick pier due to static and dynamic loading after strengthening

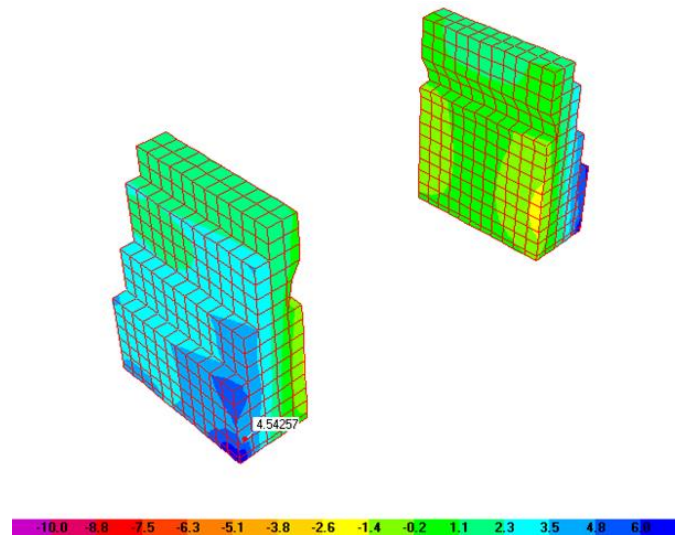


Figure 33. Maximum stresses (kg/cm^2) in the strengthened brick abutment to static and dynamic loading after strengthening

The proposed solution is also consistent with Mohamed et al. [13], who suggested increasing the raft thickness to reduce tensile stresses. Their method involves adding 1.0 m deep concrete blocks, reinforced with shear dowels between the raft and the added block, ensuring the two segments act together structurally.

The implemented strengthening measures in this study significantly improved the Regulator’s resilience. By redistributing stresses and reducing peak concentrations in vulnerable areas, the structure is now better equipped to withstand both static and dynamic forces without sustaining damage. The application of the RC jacket and increased thicknesses in key structural components mitigated potential degradation, extended the operational life of the Regulator, and reduced long-term maintenance requirements. Figures 34-a and 34-b illustrates the stress distribution in the RC jacket post-strengthening, highlighting the effectiveness of the intervention.

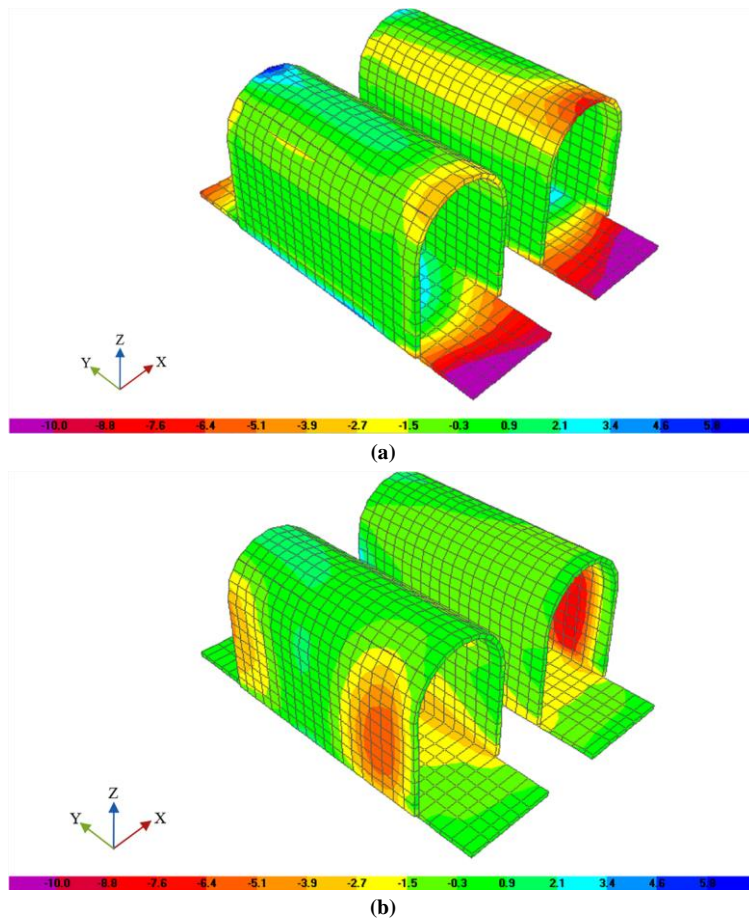


Figure 34. a) Maximum stresses (kg/cm^2) in RC jacket due to static and dynamic loading after strengthening along the x-direction, b) Maximum stresses (kg/cm^2) in RC jacket due to static and dynamic loading after strengthening along y-direction (kg/cm^2).

Table 5 and Figure 35 illustrate the maximum shear stresses (S1-2 and S1-3) in the strengthened brick mortar under static and dynamic loading conditions. The raft exhibits the highest shear stress level at 0.70 kg/cm², primarily due to its foundational role in bearing and distributing loads from the entire structure. Despite this, the stress level remains well-managed, indicating that the reinforced structure effectively handles foundational stresses. The arch displays a shear stress of 0.40 kg/cm², which represents a notable reduction compared to its original state. This reduction suggests that the reinforced concrete (RC) jacket successfully redistributes loads, minimizing stress concentrations within the arch.

Table 5. Values of shear stresses in brick mortar after strengthening

No.	Element	Material	Shear stresses (kg/cm ²)
1	Raft	Brick mortar	0.70
2	Arch	Brick mortar	0.40
3	Abutment	Brick mortar	0.35
4	Pier	Brick mortar	0.46

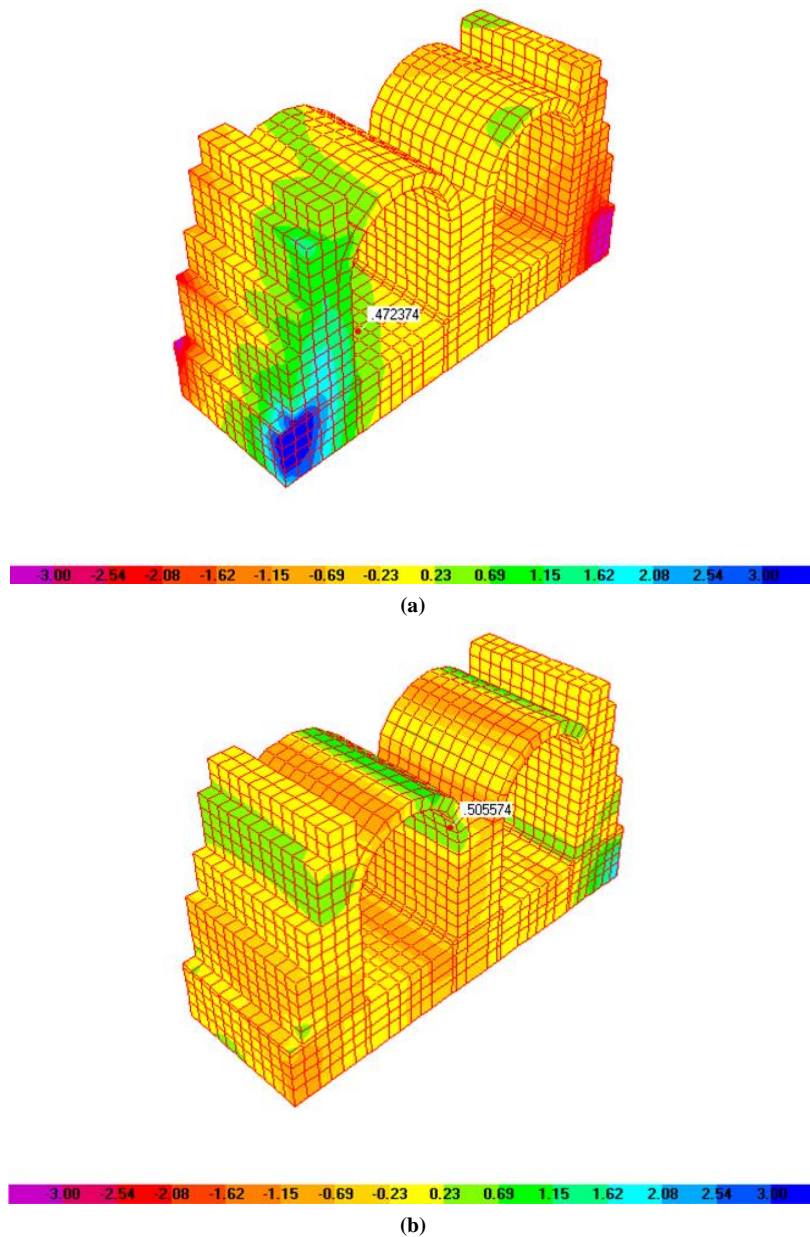


Figure 35. a) Maximum shear stresses (S1-2) in the strengthened bricks Regulator (kg/cm²) due to static and dynamic loading, b) b. Maximum shear stresses (S1-3) in strengthened bricks Regulator (kg/cm²) due to static and dynamic loading

The abutment maintains a shear stress of 0.35 kg/cm², significantly lower than its pre-strengthened levels. This improvement highlights the effectiveness of the reinforcement in enhancing the abutment's capacity to manage operational loads. Similarly, the pier exhibits a shear stress of 0.46 kg/cm², which remains within safe limits. This result

confirms that, while the pier continues to bear part of the lateral forces, it benefits from the load redistribution provided by the reinforced structure, ensuring structural stability.

Overall, the shear stress values across these components demonstrate that the strengthened Regulator now manages shear stresses more efficiently. By reducing stress concentrations and enhancing load distribution, the rehabilitation measures have significantly improved the structure's stability and resilience across critical elements.

Figure 36-a illustrates the maximum shear stress (S1-2) within the reinforced concrete (RC) jacket, measured in kg/cm², under both static and dynamic loading conditions after structural strengthening. Similarly, Figure 36-b displays the maximum shear stress (S1-3) under the same load types. These visuals provide insight into the distribution and magnitude of shear stresses post-strengthening, highlighting the RC jacket's enhanced resilience against varied loads. This improvement is crucial for maintaining stability and ensuring stresses remain within the permissible limits defined by the Egyptian Code of Practice [31], setting the context for evaluating concrete cracking stress and allowable thresholds as specified in ECP 203 standards [31].

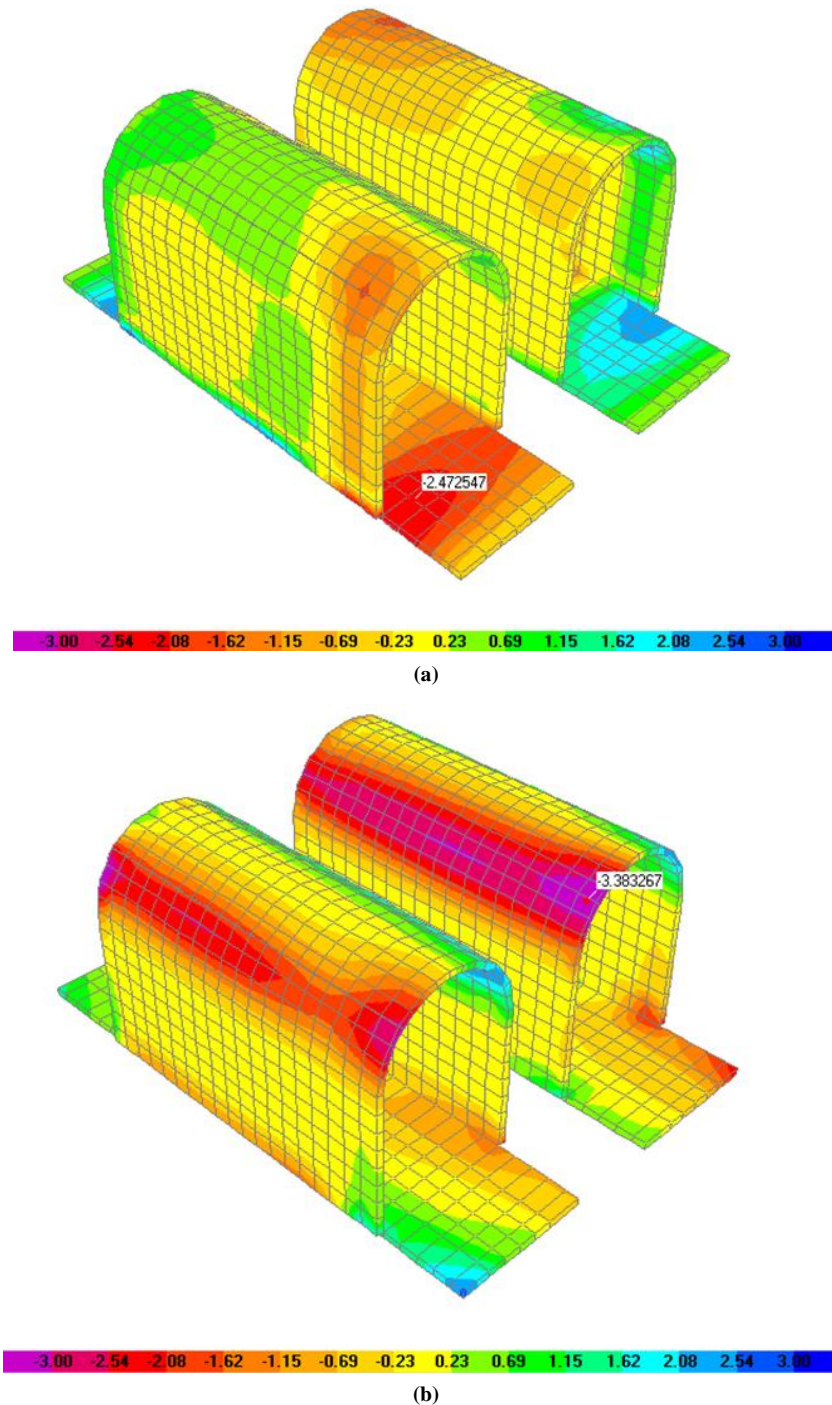


Figure 36. a) Maximum shear stresses(S1-2) in RC jacket (kg/cm²) due to static and dynamic loading after strengthening, b) Maximum shear stresses (S1-3) in RC jacket (kg/cm²) due to static and dynamic loading after strengthening

The concrete cracking stress limit according to ECP 203 [31] is calculated from the following equation (Equation 10):

$$f_{ctr} = 0.6\sqrt{f_{cu}} \quad N/mm^2 \quad (10)$$

where f_{cu} is Concrete cube strength (N/mm^2), After substitution in the equations, $f_{ctr} = 0.6\sqrt{26} = 3.06 \text{ N/mm}^2 = f_{ctr} = 30.6 \text{ kg/cm}^2$ For $t \leq 20 \text{ cm}$, $\eta\eta_1=1.0$. The allowable tension stress according to ECP 203 [31] is $f_{ct} = 30.6 \text{ kg/cm}^2$.

The tension stress for all structural RC jacket is lower than the allowable RC tension stress is $\rho_{min} = 0.15\%$ for $t \leq 200 \text{ mm}$. As = 300 mm^2 , take mesh $8 \phi 12 \text{ mm}^2 / \text{m} / \text{side}$.

The allowable compression stress according to ECP 203 [31] is (Equation 11):

$$f_c = \frac{0.67f_{cu}}{\gamma_c} \quad (11)$$

where f_{cu} Concrete cube strength, and γ_c is Partial safety factors for concrete.

After substitution in the equations: $f_c = 116 \text{ kg/cm}^2$. The compression stress for all structural RC jacket is lower than the allowable RC compressive stress. The allowable shear stress, according to ECP 203 [31] is (Equation 12):

$$q_{cu} = 0.16 \sqrt{\frac{f_{cu}}{\gamma_c}} \quad N/mm^2 \quad (12)$$

After substitution in the equation: $q_{cu} = 0.67 \text{ N/mm}^2 = q_{cu} = 6.7 \text{ kg/cm}^2$.

The shear stress for all structural RC jackets is lower than the allowable RC shear stress.

4. Comparison between Two Models

Upon comparing the stress distributions before and after the strengthening, it was observed that the stresses were effectively redistributed. The reinforced concrete jacket played a significant role in this redistribution. Unlike brick, reinforced concrete was able to handle higher stresses due to its superior strength and composite action, where the steel reinforcement works in tension. In contrast, concrete manages the compressive forces.

This redistribution of stresses meant that the reinforced concrete jacket absorbed and mitigated the stresses that were previously a concern in the brick structure. The result was a more resilient and durable Regulator capable of handling greater loads and offering improved safety and longevity.

Figures 37 and 38 illustrate the maximum compressive and tensile stresses in the brick elements before and after rehabilitation. These results were obtained from numerical models (SAP2000), where the maximum compression or tension stress at specific points in the brick elements prior to rehabilitation was compared to the corresponding stresses at the same points after rehabilitation. Figure 39 presents the maximum shear stresses in the brick mortar before and after rehabilitation. Similar to the previous results, these shear stress values were extracted from the numerical models at specific points and compared to evaluate the reduction in shear stress post-rehabilitation.

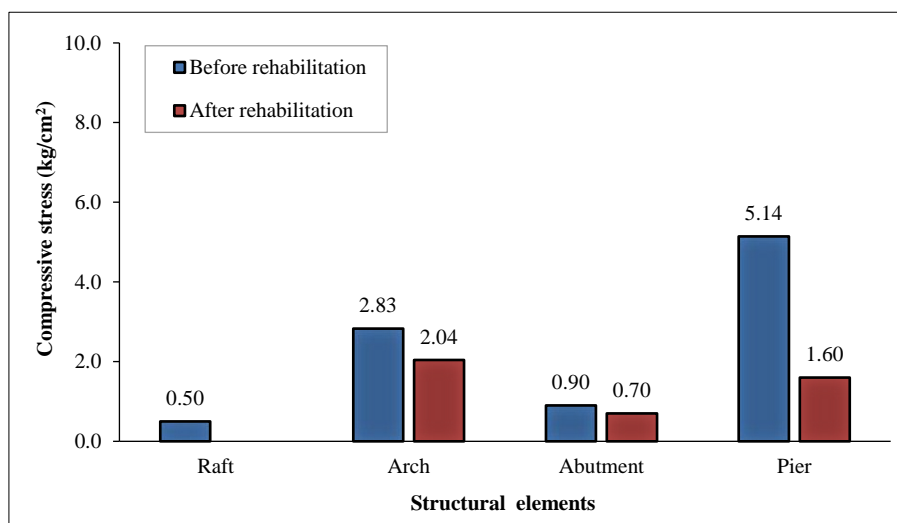


Figure 37. Maximum compressive stresses in bricks before and after rehabilitation

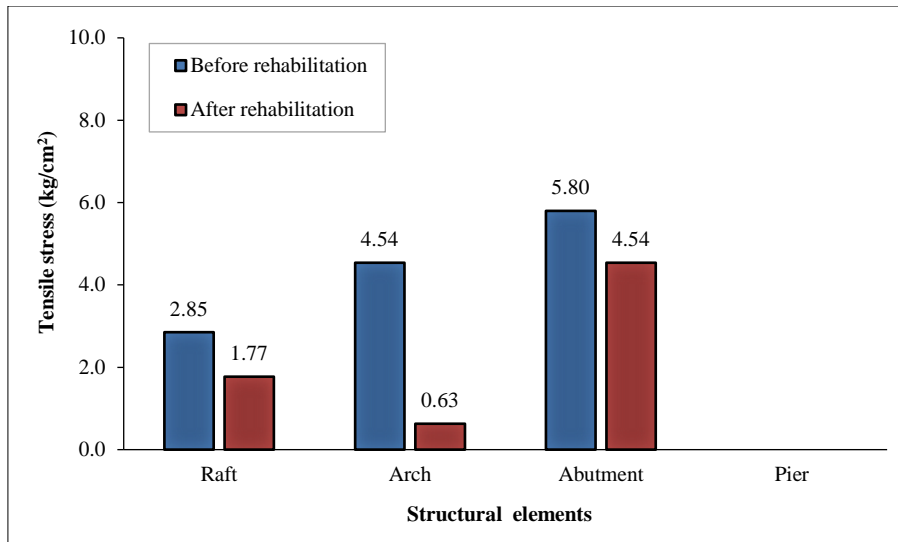


Figure 38. Maximum tensile stresses in bricks before and after rehabilitation

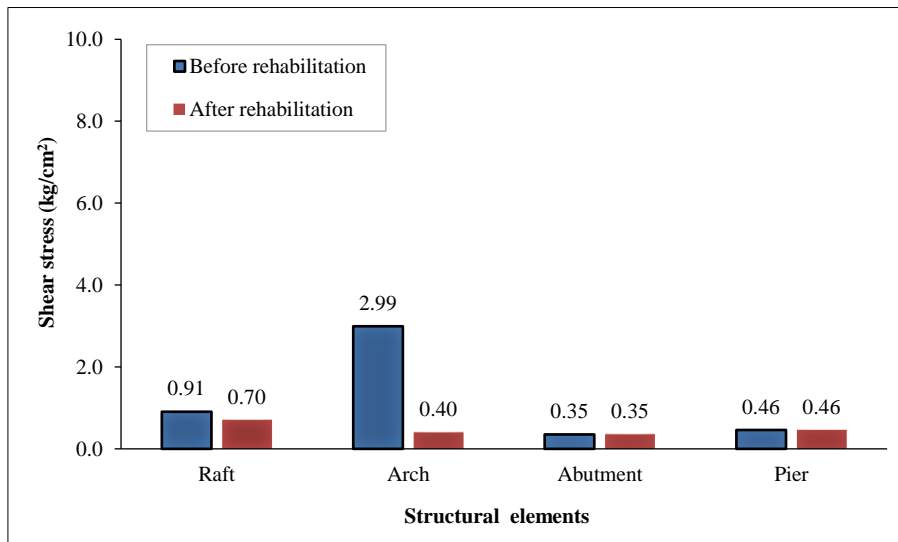


Figure 39. Maximum shear stresses in brick mortar before and after rehabilitation

Additionally, Figures 40 and 41 depict the maximum compressive and tensile stresses in the reinforced concrete (RC) jacket after rehabilitation. These stresses were obtained from the numerical models (SAP2000) at the critical points where maximum compression and tension stresses occurred.

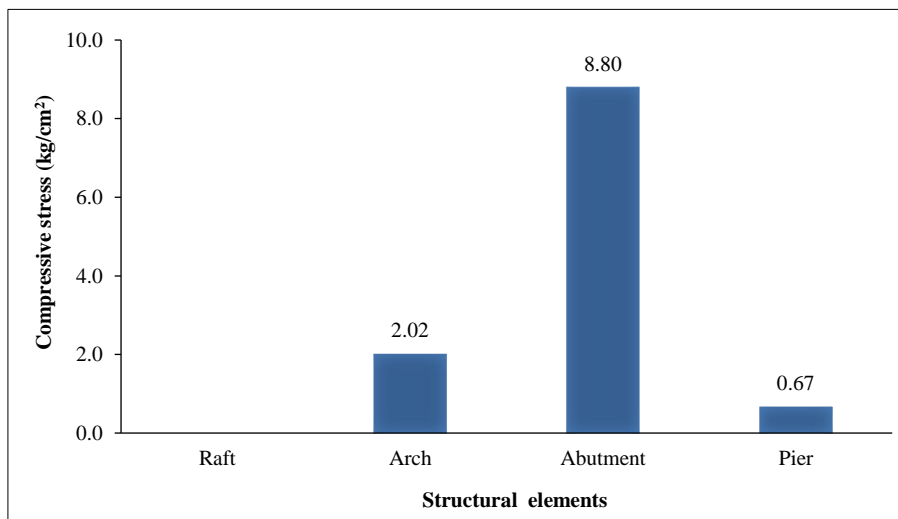


Figure 40. Maximum compressive stresses in RC jacket after rehabilitation

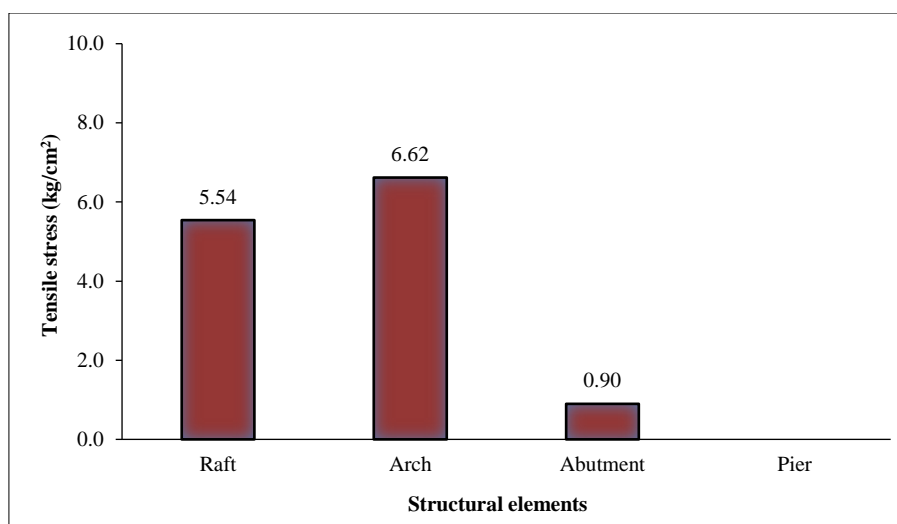


Figure 41. Maximum tensile stresses in RC jacket after rehabilitation

After rehabilitation, the brick's tensile stress decreased by 36%, 84%, and 21% for the raft, arch, and abutment, respectively. Similarly, the brick's compressive stress was reduced by 100%, 28%, 22%, and 69% for the raft, arch, abutment, and pier, respectively. The mortar's shear stress also showed significant reductions of 23% and 86% for the raft and arch, respectively. The RC jacket effectively reduced both the brick's compressive and tensile stresses across structural elements, including the arch, abutment, pier, and raft. Additionally, the RC jacket contributed to a substantial reduction in the brick mortar's shear stresses in the arch and raft, further enhancing the structural performance.

5. Conclusion

In conclusion, reinforcing the brick regulator with an internal concrete jacket has effectively improved the structural integrity of hydraulic structures. The analysis of stress distributions highlighted the benefits of utilizing reinforced concrete for managing and distributing stresses, which can significantly prolong the regulator's lifespan. This study emphasizes the importance of material assessment in heritage hydraulic structures, employing drilled boreholes for thorough evaluation. Numerical analysis accurately identified stress levels in critical sections of the regulator elements. Mechanical testing conducted over a brief period from 2015 to 2021 indicated a low deterioration rate in the materials used for the regulator. Additionally, finite element analysis has proven to be a valuable tool for identifying regions of significant stress and potential crack locations, even in submerged areas. The proposed strengthening strategy has shown effectiveness for the existing masonry structure. This includes the incorporation of reinforced concrete jackets for the piers and raft, as well as shotcrete lining for the arch. The compressive and tensile stress results of the RC jacket were lower yet consistent with the material properties and experimental findings, aligning well with the expected behavior of the material. Similarly, the brick's compressive and tensile stress values fell within acceptable ranges and were consistent with the observed material properties and experimental findings. The use of the reinforced concrete jacket significantly reduced both compressive and tensile stresses across various structural elements, as well as decreased shear stresses in the brick mortar for the arch and raft.

6. Declarations

6.1. Author Contributions

Conceptualization: A.A.M. and M.O.; methodology: A.A.M.; software: M.O.; validation: A.A.M., M.O., and D.A.E.; formal analysis: A.A.M.; investigation: M.O.; resources: D.A.E.; data curation: D.A.E.; writing—original draft preparation: A.A.M.; writing—review and editing: M.O.; visualization: D.A.E.; supervision: A.A.M. and D.A.E.; project administration: A.A.M.; funding acquisition: M.O. All authors have read and agreed to the published version of the manuscript.

6.2. Data Availability Statement

The data presented in this study are available in the article.

6.3. Funding

The authors received no financial support for the research, authorship, and/or publication of this article.

6.4. Conflicts of Interest

The authors declare no conflict of interest.

7. References

- [1] Shenouda, I. M., Fleifle, A. E., Awad, H. M., & Younan, N. A. (2018). Simulation-Optimization Model for the Hydraulic and Structural Design of Barrages-Regulators in Egypt. *Journal of Irrigation and Drainage Engineering*, 144(12), 04018034. doi:10.1061/(asce)ir.1943-4774.0001349.
- [2] Sarhosis, V., Liu, B., & Gilbert, M. (2024). The 3d response of a large-scale masonry arch bridge - part I: Performance under low and medium loading levels. *Engineering Structures*, 316. doi:10.1016/j.engstruct.2024.118496.
- [3] Diweddar, A. I., Fathy, R. M., Abd Elhamid, A. M. I., & Bahgat, M. (2023). A hybrid approach to assess the hydraulic structures rehabilitation work, case study: El-Bagoueya head regulator, Egypt. *Alexandria Engineering Journal*, 75, 67–79. doi:10.1016/j.aej.2023.05.068.
- [4] Elhakem, Y., & Emarah, D. (2022). Using Dynamic Tests to Evaluate Structural Status of Barrage Before and After Rehabilitation. *Journal of Engineering Sciences*, 17–31. doi:10.21608/jesaun.2022.151656.1156.
- [5] Anwar, A. M., & Abd Elwaly, A. M. A. (2023). Modal displacement vs Curvature functions as damage identifier for masonry structures. *Alexandria Engineering Journal*, 68, 527–538. doi:10.1016/j.aej.2023.01.042.
- [6] Liu, B., Sarhosis, V., & Lemos, J. V. (2024). Quantification of the crack propagation and global failure mechanism of single- and multi-ring masonry arch bridges. *Engineering Structures*, 306. doi:10.1016/j.engstruct.2024.117805.
- [7] Bencardino, F., Curto, R., & Scavelli, V. (2023). Inspection and Structural Rehabilitation of an Existing Masonry Arch Railway Bridge. *Applied Sciences (Switzerland)*, 13(5), 2973. doi:10.3390/app13052973.
- [8] Anwar, A. M., Hashad, A. S., & Omar, M. (2024). Dynamic measurements to assess stress levels on buried hydraulic structures. *Water Science*, 38(1), 21–32. doi:10.1080/23570008.2023.2295046.
- [9] Anwar, A. M., ELattar, A., & Abd-elwaly, A. (2022). DIM for detecting cracks in masonry piers with different crack patterns. *Journal of Engineering Sciences*, 50(6), 335-349. doi:10.21608/jesaun.2022.147021.1149.
- [10] Ramadan, A. N., Jing, P., Zhang, J., & Zohny, H. N. E. D. (2021). Numerical analysis of additional stresses in railway track elements due to subgrade settlement using fem simulation. *Applied Sciences (Switzerland)*, 11(18), 8501. doi:10.3390/app11188501.
- [11] Hamdy, G. A., El-Salakawy, T. S., El-Mashad, M. E., & Elwan, R. M. (2021). Structural Analysis and Safety Assessment of a Historic Hydraulic Structure in Egypt. *Cities' Identity Through Architecture and Arts. Advances in Science, Technology & Innovation*, Springer, Cham, Switzerland. doi:10.1007/978-3-030-14869-0_1.
- [12] da Silva, R. F. P. (2022). Advanced non-linear numerical simulation tools for in-service and retrofitting assessment of stone masonry railway arch bridges-Experimental calibration and validation. Ph.D. Thesis, University of Porto, Porto, Portugal.
- [13] Mohamed, E. K., & Khalil, E. (2018). Innovative solution for the repair of hydraulic structures (regulators). *Water Science*, 32(2), 179–191. doi:10.1016/j.wsj.2018.10.001.
- [14] Tahir, A., & Kunz, C. (2023). Reliability Based Rehabilitation of Existing Hydraulic Structures. *Proceedings of PIANC Smart Rivers 2022, PIANC 2022, Lecture Notes in Civil Engineering*, 264, Springer, Singapore. doi:10.1007/978-981-19-6138-0_50.
- [15] Brachaczek, W., & Gałuszka, A. (2023). Repair of concretes in the underwater part of a water barrage. *Energy Optimized Construction*, 12, 116–123. doi:10.17512/bozpe.2023.12.13.
- [16] Bianchini, N., Sabra, Z., Green, K., & Wright, R. (2024). In-situ testing and modeling of a masonry bridge in Surrey (UK): Waverley Mill bridge. *Procedia Structural Integrity*, 64, 352-359. doi:10.1016/j.prostr.2024.09.262.
- [17] Erduran, E., Gonen, S., Pulatsu, B., & Soyoz, S. (2023). Damping in masonry arch railway bridges under service loads: An experimental and numerical investigation. *Engineering Structures*, 294. doi:10.1016/j.engstruct.2023.116801.
- [18] kashani, H. K., Shakiba, M., Bazli, M., Hosseini, S. M., Mortazavi, S. M. R., & Arashpour, M. (2023). The structural response of masonry walls strengthened using prestressed near surface mounted GFRP bars under cyclic loading. *Materials and Structures/Materiaux et Constructions*, 56(6), 112. doi:10.1617/s11527-023-02201-0.
- [19] Zampieri, P., Simoncello, N., Tetougueni, C. D., & Pellegrino, C. (2018). A review of methods for strengthening of masonry arches with composite materials. *Engineering Structures*, 171, 154–169. doi:10.1016/j.engstruct.2018.05.070.
- [20] Anwar, A. M. (2015). Performance of Masonry Arches Strengthened With CFRP Sandwich. *Journal of Engineering Sciences*, 43(6), 823–836. doi:10.21608/jesaun.2015.115296.
- [21] Alecci, V., De Stefano, M., Focacci, F., Luciano, R., Rovero, L., & Stipo, G. (2017). Strengthening masonry arches with lime-based mortar composite. *Buildings*, 7(2), 49. doi:10.3390/buildings7020049.
- [22] Simoncello, N., Zampieri, P., Gonzalez-Liberos, J., & Pellegrino, C. (2019). Strengthening of Masonry Arches with SFRM. *Key Engineering Materials*, 817, 244–250. doi:10.4028/www.scientific.net/kem.817.244.

- [23] Elsayed, A. Abdel-Z., Aly, A. G., Ahmed, M. H., & Omran, O. A. E. (2012). Repair and Strengthening of the Water Piers Barrages By Injection Technique and Its Evaluation. *JES. Journal of Engineering Sciences*, 40(1), 1–19. doi:10.21608/jesaun.2012.112330.
- [24] Ballivy, G., Perret, S., Rhazi, J., Palardy, D., Laporte, R., & Gagnon, E. (2001). Rehabilitation of hydraulic masonry heritage structures: Injection of special cement-based grouts and tomographic control. *WIT Transactions on the Built Environment*, 55, 527–536.
- [25] Jiang, Z., Yang, J., & Su, H. (2023). Mechanical response of masonry structure strengthened with ultra-high performance concrete (UHPC): a comparative analysis for different strengthening tactics. *Frontiers in Materials*, 10. doi:10.3389/fmats.2023.1289225.
- [26] Zampieri, P., Piazzon, R., Niero, L., & Pellegrino, C. (2024). Damaged masonry arch bridges strengthened with external post-tensioning: Experimental and numerical results. *Engineering Structures*, 318. doi:10.1016/j.engstruct.2024.117929.
- [27] Anwar, M., Anwar, A. M., & Emarah, D. A. (2023). Structural Assessment of Heritage Hydraulic Structures - Case Study. *Proceedings of the 3rd International Conference on Civil Engineering (ICCE2023)*, 24-27 October, 2023, Hurghada, Egypt.
- [28] Ionescu, B., Hegyi, A., Lăzarescu, A., & Mircea, A. C. (2019). A review regarding the sustainable use of shotcrete at national and international level. *Constructii*, 20(1/2), 57-64.
- [29] Liu, G., Zhao, J., Zhang, Z., Wang, C., & Xu, Q. (2021). Mechanical properties and microstructure of shotcrete under high temperature. *Applied Sciences (Switzerland)*, 11(19). doi:10.3390/app11199043.
- [30] ECP201. (2012). Egyptian code for calculating loads and forces in construction and building works. Housing and Building National Research Center, Cairo, Egypt.
- [31] ECP203. (2020). Egyptian Code for the Design and Implementation of Concrete Structures. Housing and Building National Research Center, Cairo, Egypt.
- [32] ECP202. (2005). Egyptian code for soil mechanics—Design and construction of foundations. Housing and Building National Research Center, Cairo, Egypt.
- [33] CSI. (2010). SAP2000, Version 14.2.2. Computers and Structures Inc. (CSI), Viale Lombardia, Italy.
- [34] Calderini, C., Lagomarsino, S., Rossi, M., De Canio, G., Mongelli, M. L., & Roselli, I. (2014). Shaking table tests of an arch-pillars system and design of strengthening by the use of tie-rods. *Bulletin of Earthquake Engineering*, 13(1), 279–297. doi:10.1007/s10518-014-9678-x.
- [35] Alecci, V., Focacci, F., Rovero, L., Stipo, G., & De Stefano, M. (2016). Extrados strengthening of brick masonry arches with PBO–FRCM composites: Experimental and analytical investigations. *Composite Structures*, 149, 184–196. doi:10.1016/j.compstruct.2016.04.030.
- [36] Alecci, V., Focacci, F., Rovero, L., Stipo, G., & De Stefano, M. (2017). Intrados strengthening of brick masonry arches with different FRCM composites: Experimental and analytical investigations. *Composite Structures*, 176, 898–909. doi:10.1016/j.compstruct.2017.06.023.
- [37] Carozzi, F. G., Poggi, C., Bertolesi, E., & Milani, G. (2018). Ancient masonry arches and vaults strengthened with TRM, SRG and FRP composites: Experimental evaluation. *Composite Structures*, 187, 466–480. doi:10.1016/j.compstruct.2017.12.075.
- [38] Gattesco, N., Boem, I., & Andretta, V. (2018). Experimental behaviour of non-structural masonry vaults reinforced through fibre-reinforced mortar coating and subjected to cyclic horizontal loads. *Engineering Structures*, 172, 419–431. doi:10.1016/j.engstruct.2018.06.044.
- [39] Oliveira, D. V., Basilio, I., & Lourenço, P. B. (2010). Experimental Behavior of FRP Strengthened Masonry Arches. *Journal of Composites for Construction*, 14(3), 312–322. doi:10.1061/(asce)cc.1943-5614.0000086.
- [40] Zampieri, P. (2020). Horizontal capacity of single-span masonry bridges with intrados FRCM strengthening. *Composite Structures*, 244, 112238. doi:10.1016/j.compstruct.2020.112238.